7-2014

The Photophysical Properties of Squaraine Derivatives and Their Impact upon Photovoltaic Efficiencies

Bi Zhu

The Photophysical Properties of Squaraine Derivatives and Their Impact upon Photovoltaic Efficiencies

Bi Zhu

B.S. Chemistry, Beijing Institute of Technology, Beijing, China, 2010

A thesis submitted in partial fulfillment of the
requirements for the degree of Master of Science in Chemistry in the
School of Chemistry and Materials Science,
College of Science
Rochester Institute of Technology

July 2014

Signature of the Author Bi Zhu

Accepted by Joseph Hornak 9/10/2014
Director, M.S. Degree Program Date

SCHOOL OF CHEMISTRY AND MATERIALS SCIENCE
COLLEGE OF SCIENCE
ROCHESTER INSTITUTE OF TECHNOLOGY
ROCHESTER, NEW YORK

CERTIFICATE OF APPROVAL

M.S. DEGREE THESIS

`

The M.S. Degree Thesis of Bi Zhu has
been examined and approved by the thesis
committee as satisfactory for the thesis required for
the M.S. degree in Chemistry.

_____
Dr. Christopher J. Collison, *Thesis Advisor*

_____
Dr. Christiaan P. Richter

_____
Dr. Jeremy Cody

_____
Dr. Scott Williams

_____
Date

Acknowledgements

I would like to express my special appreciation and thanks to my advisor Professor Dr. Christopher J. Collison. I would like to thank him for encouraging my research and for allowing me to grow as a research scientist. I am deeply indebted to him for his support and commitment, his enthusiastic guidance, and his insight throughout the research. He could not have been more generous with his time and effort in directing me toward the completion of my thesis. I would also like to thank my committee members, Professor Christiaan Richter, Professor Scott Williams, and Professor Jeremy Cody for serving as my committee members even at hardship. As my research has been largely carried out in the Department of Chemistry and Nano Science, I would therefore like to profusely thank the faculty, staff, and fellow students whose contributions were always tremendously helpful and illuminating to me.

Abstract

Squaraine dyes provide potential on improving the efficiency of Organic photovoltaic OPV solar cell. Characterization of the photophysical properties of squaraine dyes is going to help us find the best material for our device. A series of squaraines ($DESQ(OH)_2$, $DiBSQ(OH)_2$, and novel $DiPSQ(OH)_2$) in which side chains length increasing were characterized in this paper. The material photophysical properties of these squaraines were systematically characterized using various tools. Our research showed that the length of side chain plays an important role in aggregation properties of squaraines, longer side chains result in smaller exciton splitting and hence less broadened absorbance spectrum. Interestingly, $DiPSQ(OH)_2$ which has the longest side chains unexpectedly gave the most broadened absorbance spectrum in aggregation. The impact of aggregation on fluorescence was also studied, we demonstrated that the squaraines lost fluorescence before a pure solid state was reached. We attribute this to the formation of some kind long range aggregate.

Contents

Chapter 1

Introduction

1.1 Organic Photovoltaic Solar Cell

The fact that fossil fuels will someday exhaust stimulates scientific research for inexpensive sustainable energy sources, such as ideal efficient, low-cost photovoltaic devices.[1] The organic, polymer-based photovoltaic elements have introduced the potential of obtaining cheap and easy methods to convert electrical energy from light.[2] Organic photovoltaic (OPV) cells are cheap, easy to make, flexible and tunable in wavelength responsiveness. However, the commercial value of the OPV cell depends on its efficiency, which is low and currently limits the wide spread use of OPV.

The general structure used for organic solar cells is in a sandwich geometry (***figure 1.1***). Substrates typically used are glass or plastic, each covered with a conducting electrode (anode) such as ITO (indium tin oxide). The active layer which comprises a mixture of electron acceptor and donor is coated using spin cast or vacuum deposition techniques. Finally the top electrode (metal cathode) is evaporated. In general, a lower work-function metal (as compared to ITO) such as aluminum is used.[3]

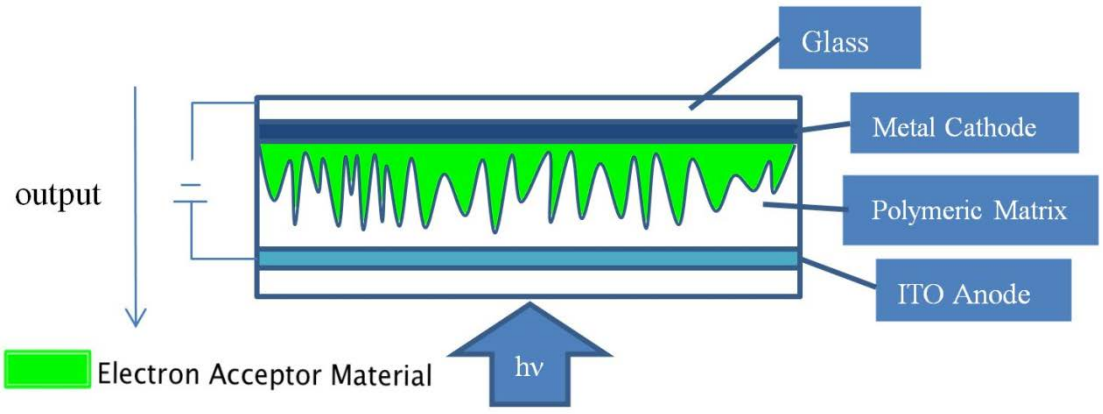

Figure 1.1: general structure of organic solar cells.

The process of conversion of light into electricity by an organic solar cell can be simply and schematically described by the following steps: (1) organic dyes absorb a

photon and form an excited state, this step is known as exciton (excited state electron and the bound hole pair) creation (***figure 1.2***);

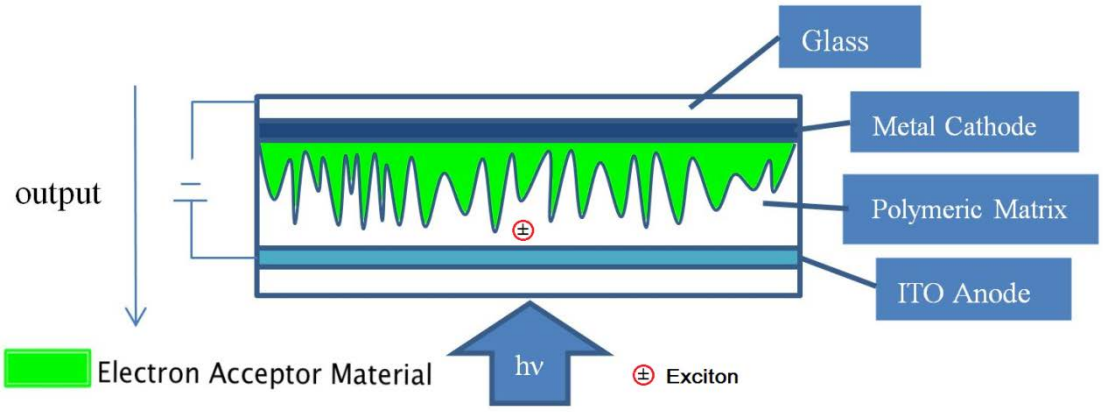

Figure 1.2: exciton creation.

(2) The exciton diffuses to the interface of the electron donor and the electron acceptor where exciton dissociation can now take place, this migration of the bound electron-hole pair is known as exciton diffusion (***figure 1.3***);

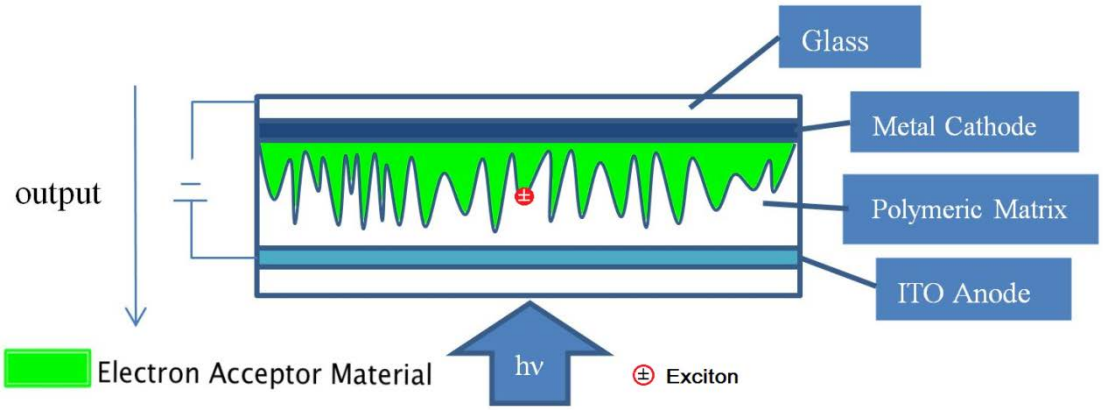

Figure 1.3: exciton diffusion.

(3) The bound electron-hole pair dissociates into free charges, this step is known as charge separation (***figure 1.4***);

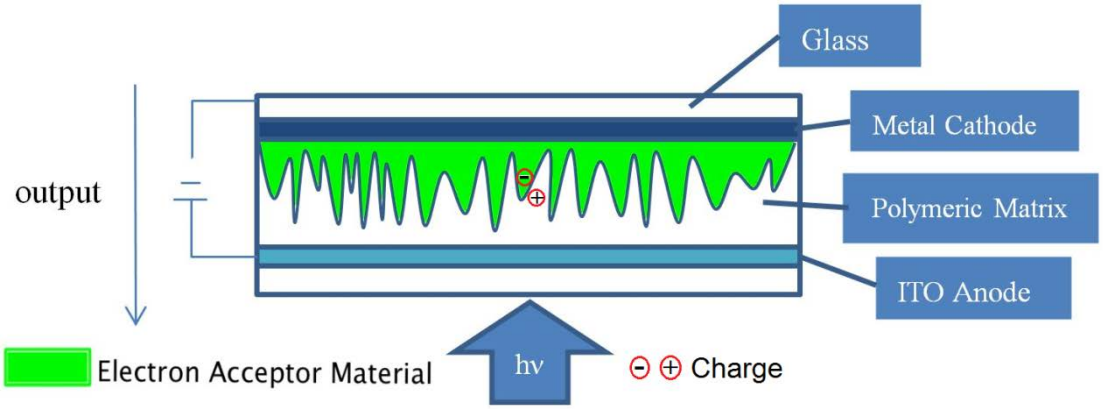

Figure 1.4: charge separation.

and (4) charge is transported within the organic semiconductor to the respective electrodes, this step is known as charge collection (***figure 1.5***).[4]

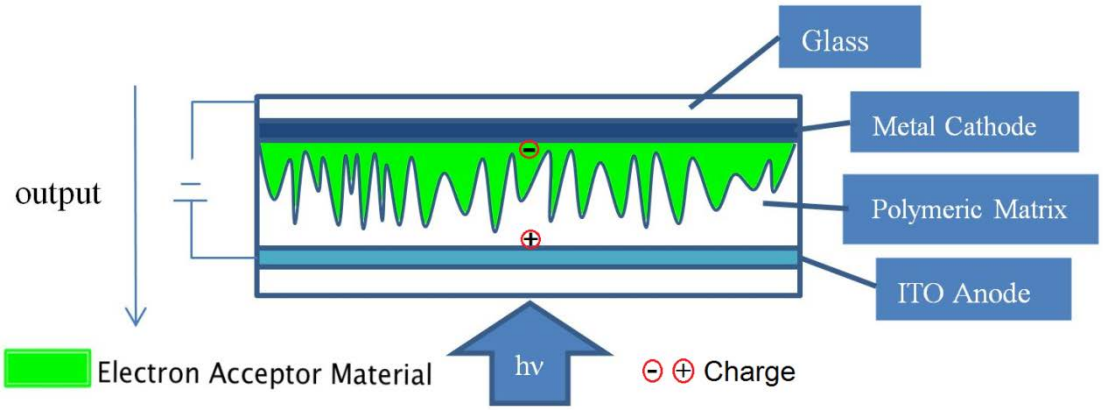

Figure 1.5: charge collection.

Organic photovoltaic solar cells function in a mechanism that is different from conventional solar cells.[5] In conventional photovoltaic cells both electrons and holes coexist in the same chemical phase (say, *p*-type material). Their efficiencies are determined primarily by the ability of photogenerated minority carriers (excited electron) to escape from, say, the *p*-type region of the device before recombining with the majority carriers. The crucial processes of photogeneration, separation and recombination of charge carriers all occur primarily in the bulk material, i.e. crystalline silicon. Therefore, bulk properties such as crystallinity and chemical purity often control the efficiency of conventional solar cells, and optimizing these properties can be expensive.[6] Organic photovoltaic solar cells, on the other hand, are a special class of devices in which a photon is absorbed by a photosensitive dye molecule. Charge carriers are generated (and simultaneously separated) at the heterointerface by exciton

dissociation. This interfacial mode of carrier generation is fundamentally different from the bulk generation occurring in conventional cells, which make bulk properties less critical. At some level, this allows less pure and therefore less expensive materials to be used.

The efficiency of organic photovoltaic solar cells can by predicted by ***equation 1.1***:

$$\eta_{OPV} = \eta_A \eta_{ED} \eta_{CT} \eta_{CC} \quad \textbf{(Equation 1.1)}$$

In which η_{OPV} is the efficiency of the OPV cell, η_A, η_{ED}, η_{CT}, and η_{CC} are the efficiencies of absorption, exciton diffusion, charge transfer, and charge collection, respectively. Although the efficiencies of all these operations impact the overall efficiency of the device, the efficiencies of absorption and exciton diffusion and their correlation with the structure of the organic dye molecule is addressed in this thesis.

The absorption efficiency, η_A, is determined by the extinction coefficient ε and the range of the absorption spectrum. To optimize the absorption efficiency, the ideal organic dye is expected to have a high extinction coefficient and a wide absorption range. The exciton diffusion efficiency, η_{ED}, is determined by ***equation 1.2***[7].

$$\eta_{ED} = e^{-d/L_D} \quad \textbf{(Equation 1.2)}$$

In which d is the distance the exciton must travel to the interface where charge transfer takes place and L_D is the exciton diffusion length. The exciton diffusion length depends both on the rate of diffusion and the lifetime of the exciton. It is claimed[8] that in most cases the efficiency of an OPV device is limited by the efficiency of exciton diffusion. To increase the efficiency of exciton diffusion, it is crucial to increase the length of exciton diffusion, which means increasing the rate of diffusion and the lifetime of the exciton. While the excited state life time is believed to be an inherent property of a molecule, the rate of exciton diffusion depends upon molecular packing and the extent of crystallinity. It is vital to characterize new organic dye materials for photophysical properties and morphological properties in a thin film, so that efficiencies can be proved to be correlated with these variables.

1.2 Squaraine Dyes

Squaraine dyes (***figure 1.6***) are a novel class of organic dyes, which have high extinction coefficients, sharp absorption bands, and intense fluorescence spectra in the red and near infrared region in solution.[9] The "squaraine", whose name was proposed by Schmidt in 1981,[10] is characterized by the unique aromatic four-membered carbon ring system.

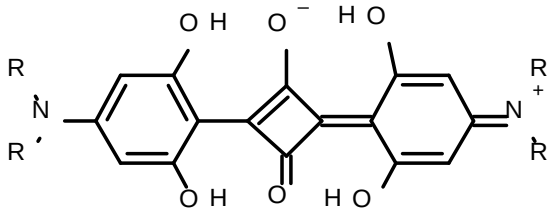

D—A—D

Figure 1.6: general structure for squaraine dyes.

Based on MNDO and CNDO semiempirical molecular-orbital (MO) calculations by Bigelow and Freund[11], the electronic structure of squaraines is described with donor-acceptor-donor (D-A-D) charge transfer (CT) states at both ground state and excited state. The electron donor groups are the two anilino groups on both sides and the electron acceptor is the central four-membered ring. According to Bigelow and Freund, the CT of squaraines is mainly confined between the central four membered carbon ring and the oxygen atoms.[12] Although in solution squaraines have similar sharp absorption bands, their absorption spectra in the solid state are very broad and varied. The unique electronic structure and such optical characteristics have made squaraines very attractive for many device applications,[9] such as xerographic photoreceptors, [13] organic solar cells, [14] optical recording media, [15] electro-luminescence diodes,[16] and nonlinear optical devices.[17] In this thesis three novel squaraines are characterized as a prerequisite for application in organic photovoltaic (OPV) devices.

Squaraine dyes are chosen as materials for OPV devices because: (1) they are

thermally stable[18] and stable towards light[19]; (2) the high extinction coefficients of squaraine dyes in the NIR region offer a potential to absorb in the near infrared region of the solar spectrum, which is not absorbed by today's best active layer materials such as P3HT[20]; (3) by changing the side group (R groups), one can tune the chemical and photophysical properties of squaraine dyes as well as impact the morphology of the film.

The broadening of the absorption spectra of squaraines in the solid state is another beneficial feature for OPV devices because an ideal solar cell is expected to absorb solar radiation over as broad a range as possible. This means a high extinction coefficient over a large range of wavelengths is desirable. Despite the photophysical properties of squaraines not changing much in solution as the R group changes, their absorption in the solid state is highly dependent upon this changing R-group, in particular because of different aggregation patterns, likely influenced by the nature of the side N-alkyl group. The ways of broadening and shifting are different because of different aggregate patterns which are controlled by different side groups. We hypothesize that aggregation of squaraines is crucial to OPV devices because it will change a lot of properties that matter for the efficiency of OPV, such as the absorption band, the extinction coefficient, the excited state life time, and the exciton diffusion length.

1.3 Aggregate of squaraines

The absorption spectra of squaraine dyes in the solid state (thin film) are different from those measured in solution in the aspect of broadening shape and shifted peak position (***figure 1.7***). This phenomenon is based upon the self-association of squaraine molecules which results from the strong intermolecular force between the molecules.

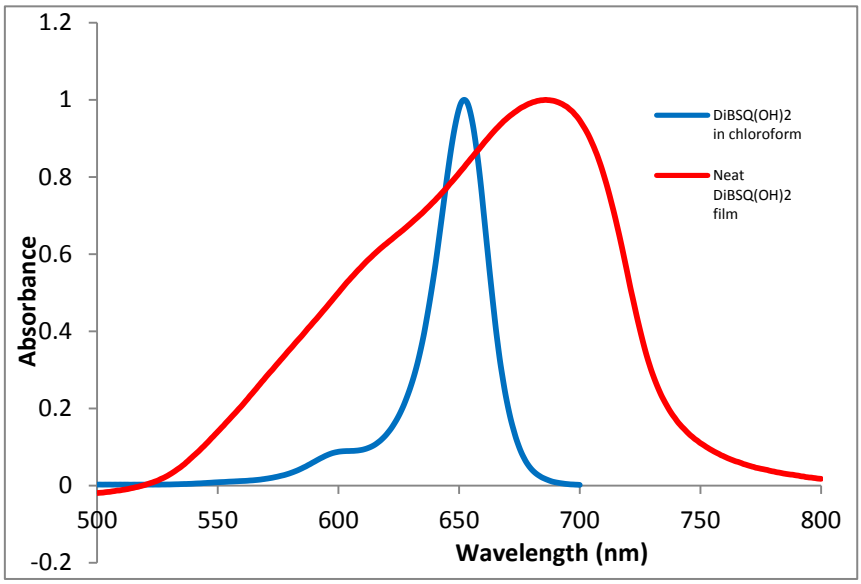

Figure 1.7: Absorption spectra of $DiBSQ(OH)_2$ squaraine when no aggregation (blue line) and aggregation happens (red line).

Although various aggregate absorption bands have been discovered on dyes in different media, they can be generated into two different types based on whether a red shift or blue-shift is observed compared with the monomer band typical of solution spectra. The aggregates that exhibit bathochromically shifted (red-shifted) bands in absorption spectra are called J-aggregates while others that exhibit hypsochromically shifted bands are called H-aggregates. Such two different kinds of shifted absorption bands of aggregates have been explained in terms of molecular exciton coupling theory, which describes the coupling of transition moments of aggregated dye molecules[21].

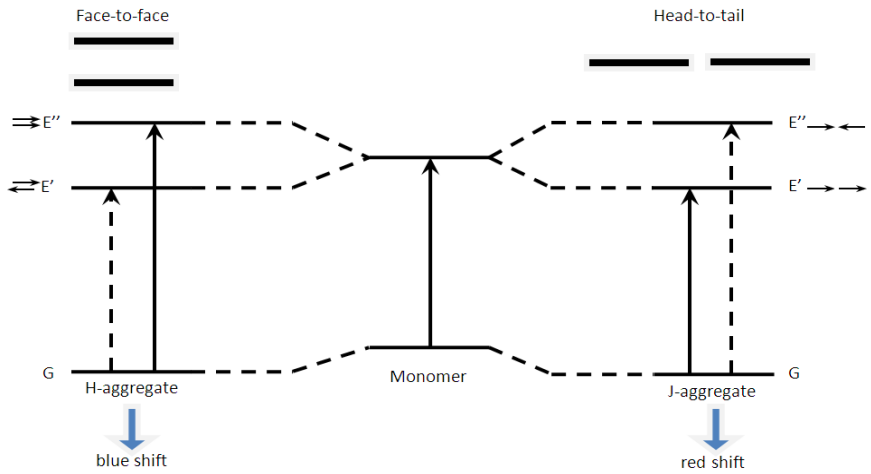

Figure 1.8: Exciton energy level diagram of H-aggregate and J-aggregate.

Extensive research on aggregates has revealed that molecules stack in a parallel form in both H- and J-aggregates (***figure 1.8***). According to exciton theory each dye

molecule is treated as a point dipole. When molecules stack together the excited state of the dimer splits into two levels (E' and E'') due to the interaction of the transition dipoles. In H-aggregates, dye molecules stack face-to-face to form a sandwich type arrangement. Molecules may also stack in a head-to-tail (end-to-end) arrangement to form a J-aggregate. The arrows in ***figure 1.8*** indicate the vector of transition dipoles and transitions are allowed only when the sum of vector is not zero. Since dye molecules in this simplified model are parallel with each other, that means transitions are only allowed when two vectors face the same direction (solid line) and forbidden when two vectors are opposite (dashed line). In the H-aggregate, the transition from the ground state to the excited state E'', which is in a higher energy level due to the repulsion of dipoles, is allowed, leading to the hypsochromic (blue) shift of absorption band. In the J-aggregate, on the other hand, the transition from ground state to a lower excited state E' is allowed, leading to the bathochromic (red) shift.

1.4 Quenching

Fluorescence quenching refers to the process which leads to the decreases in fluorescence intensity (quantum yield) of a given substance. Quenching results from a variety of molecular interactions, such as excited-state reactions, molecular rearrangements, energy transfer, ground state complex formation, and collisional quenching.[22] In general, quenching occurs without any permanent change in the molecules, that is, without a photochemical reaction. Collisional quenching happens when an excited molecule (M*) reacts with any other molecule (quencher) in a mechanism of collisional encounters and returns to the ground state through a nonradiative process.[23] Static quenching is also a valuable source of information about binding between the fluorophore and the quencher. Studies on the process of quenching could be complicated in the data analysis since multiple mechanisms of quenching may happen at the same time.[22]

Although a wide variety of substances act as quenchers of fluorescence, the subject of this paper, the squaraines, are only blended with PCBM. Hence there are only two kinds of quenchers that will be discussed: PCBM and squaraine itself (self-quenching). Fluorescence quenching is studied both as a fundamental phenomenon and a source of information about the OPV device. Chemical studies of quenching can provide information about the molecular interactions of squaraines and PCBM which is crucial for the efficiency of the OPV device. Both static and collisional quenching require molecular contact between the fluorophore and quencher. In the case of collisional quenching, the quencher and fluorophore must contact each other by diffusion during the lifetime of the excited state. Upon contact, the fluorophore returns to the ground state, without emission of a photon. In static quenching, on the other hand, a ground-state complex is formed between the fluorophore and the quencher, and this complex is nonfluorescent. When this complex absorbs light it immediately returns to the ground state without emission of a photon (***figure 1.9***).

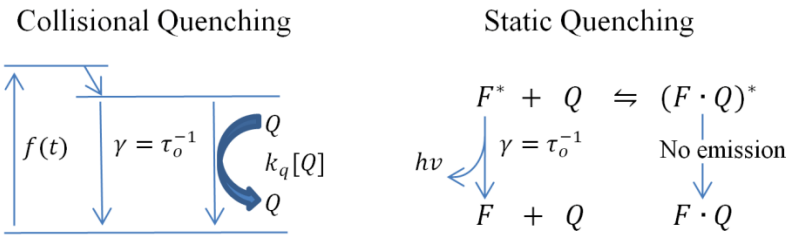

Figure 1.9: Comparison of dynamic and static quenching.

For either static or dynamic quenching to occur the fluorophore and quencher must be in contact. The requirement of molecular contact for quenching makes quenching a powerful tool to research the interactions between molecules. Quenching measurements can reveal the accessibility of fluorophores to quenchers. Considering the organic photovoltaic cell is in the form of a thin film device, this dissertation also addresses the effect of quenching in the solid state. A squaraine molecule can be considered as a fluorophore bound either to PCBM or to squaraine itself. Squaraine could bind with PCBM, or with another squaraine molecule to allow self-quenching. The quenching rate of these two kinds of quenching is expected to be different due to the different properties of the squaraine-squaraine dimer and the squaraine-PCBM

complex. If the squaraine does not combine with PCBM to form a static complex, then the quantum yield of squaraine in thin film should not significantly change after blending with PCBM. If squaraine does quench with PCBM then the quenching will be more complex because now the quenching with PCBM or another squaraine molecule will be competitive. For this reason, quenching studies might be used to reveal the morphology of a squaraine: PCBM thin film, and the permeability of energy transfer from squaraine to PCBM. Also the question exists as to whether PCBM binds with squaraines in solution before spin casting and annealing experiments can be used to test this hypothesis.

1.5 Side groups impact aggregations

As described in ***figure 1.8***, the way of molecules packing determines whether it is H-aggregation (face-to-face) or J-aggregation (head-to-tail). It has been reported that aggregation could enhance exciton diffusion length through enhanced crystalline order and exciton mobility.[24, 25] Since exciton diffusion length ($\boldsymbol{L_D}$) is crucial for OPV devices (***equation 1.2***), a better understanding of photophysical properties of aggregation itself could be helpful in optimizing the efficiency of OPV devices.

N-alkyl side groups impact aggregation by disturbing the intermolecular CT state between the anilino moiety and the central C_4O_2 unit of squaraine due to steric hindrance. Wingard has proposed that the broad absorption observed in the solid state is a direct consequence of the intermolecular charge-transfer interaction. [26] Tristani-Kendra and Eckhardt made a similar conclusion in their study.[27] Law did further research and reported that the splitting between monomer band and aggregate band become smaller as the length of side groups increases.[13] As the length of side groups grows, we expect to see a smaller splitting on the absorbance band in solid state due to increasing steric hindrance in aggregation.[13] To test this hypothesis, study on photophysical properties of squaraines will be performed in a blend of PMMA thin

films, which can be considered as solid state solutions. We expect to see squaraines possess identical properties as in liquid solution in a region of low concentration, and aggregate when concentration is high. This is to say, we expect to see a mixture of monomer and aggregate in such kind of solid solutions. The extent of aggregation should be able to be controlled by the concentration of squaraines; this feature might let us study the photophysics of both monomer and aggregate at the same time. Furthermore, if PCBM was added to such PMMA films, the impact of the quenching effect could also be studied in solid solutions. With both PCBM and squaraines blended in a same film, we might investigate and compare the relative fluorescence quenching of PCBM with self-quenching of squaraines.

Understanding the photophysics of squaraine is important, since organic photovoltaic devices (OPV) work with a mechanism fundamentally different from conventional inorganic photovoltaic devices (IPV).[28] In OPV cells light is absorbed by the organic dye molecules, which results primarily in the production of excitons (mobile excited states) rather than free electron-hole pairs. In order to produce a efficiently working OPV device, excitons must diffuse to an interface for Charge-Separation (***figure 1.4***) as much as possible. By investigating the photophysics of the excited state, we can start draw conclusions about those properties that are crucial for the efficiency of OPV, particularly on exciton diffusion and rate of photo-induced charge transfer at the bulk heterojunction interface. Ultimately when we learned how the excited state limits the efficiency of a device we can predict what changes we must make in the molecules to improve the efficiency of OPV.

1.6 Introducing a novel squaraine

To optimize the structure of squaraine for usage of fabricating OPV devices, Minquan Tian et al have synthesized a series of squaraines, including $DESQ(OH)_2$ (***figure 1.10a***) and $DiPSQ(OH)_2$ (***figure 1.10b***), and studied their properties.[29] As a

result, squaraines with four hydroxyl groups at the 2′,6′-positions of the two phenyl rings have much better thermal stability than those which have only two hydroxyls at the same 2′-positions. Furthermore, Minquan Tian et al have demonstrated that longer straight *N*-alkyl chains give larger steric hindrance than the shorter ones, and the branched *N*-alkyl chains such as isobutyls give even larger steric hindrance than the straight ones. Owing to the strong steric hindrance, the branched N-alkyl chain greatly suppresses the formation of H-aggregates and facilitates the formation of J-aggregates in thin films, which gives some selectivity on H- and J- aggregates.[29] In summary, squaraines with four hydroxyl groups and branched N-alkyl chains are ideal for thin film coating and hence may find application in fabrication of OPV devices.

To further study the effect of varying the length of side N-alkyl chains on the properties of squaraines, particularly on aggregation a new squaraine is synthesized by RIT's Dr. Cody, $DiPSQ(OH)_2$ (***figure 1.10c***). Like $DiBSQ(OH)_2$, it has four hydroxyl groups and branched N-alkyl chains. The only difference between $DiBSQ(OH)_2$ and the novel $DiPSQ(OH)_2$ is the length of N-alkyl side groups; in $DiPSQ(OH)_2$ they are isopentyls, which is one carbon atom longer than the isobutyls in $DiBSQ(OH)_2$. Now that a series of squaraines exists in which the only variation is the length of the side N-alkyl chains, the impact of the length of side groups could be studied.

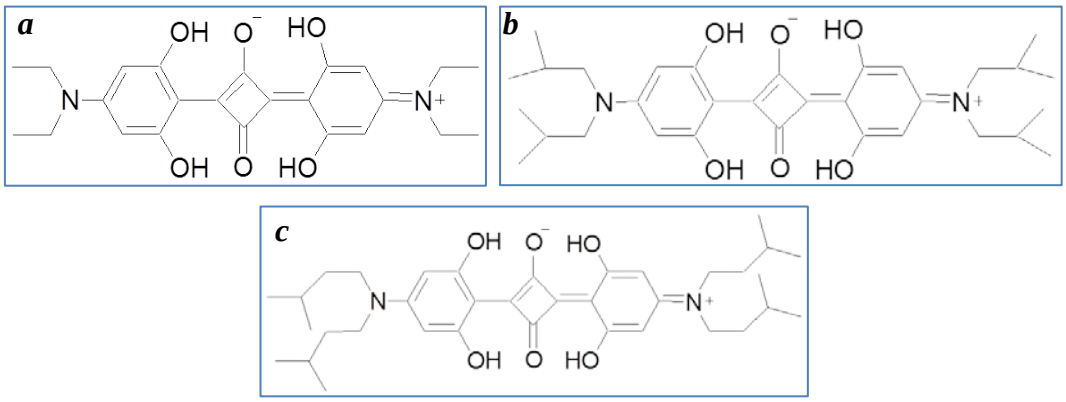

Figure 1.10: Molecular structure of (***a***)$DESQ(OH)_2$, (***b***)$DiBSQ(OH)_2$, (***c***)$DiPSQ(OH)_2$.

Chapter 2

Experiments

2.1 Sample Preparation

All samples of squaraine solutions were prepared in 20mL glass scintillation vials. Stock solutions were sonicated for 20 minutes at power level 9 in a VWR bath sonicator (model 750). All the samples were kept in a dark drawer. The volumes of solutions were measured by VWR micropipettes. Solutions were transferred by VWR Pasteur Pipet unless stated otherwise.

All the films were coated with a Chemat spin coater (model KW-4A) on the substrate of VWR microscope slides, cut into 1 inch squares. In order to coat PMMA films, solutions of squaraine and PMMA in chloroform were prepared first. For all the films, solutions were freshly prepared and were sonicated for 20 minutes before spin casting. The spin speed and time were varied depending on the concentration of PMMA, ranging from 700RPM to 1000RPM, 10 seconds to 30 seconds, respectively.

2.2 Spectroscopy

Both absorbance and fluorescence spectroscopy are applied on three squaraines. All measurements on solution were made using 10mm quartz spectrum cells (type 23/Q/10) for both absorbance and fluorescence. Measurements of fluorescence on thin films were made using a film holder. All measurements were made at room temperature.

Absorbance measurements were made on a Shimadzu UV-2401 PC UV recording spectrophotometer. The instrument parameters were set at medium scan speed, 0.5nm slit width, and 1nm sampling interval for all the samples. The scan range varies depending on solvent and solute in the sample.

Fluorescence measurements were made on a Horiba Jobin Yvon Fluoromax-4 spectrofluorometer. The integration time is always maintained at 0.1s; the wavelength of excitation is varied in order to obtain best spectra. The slit width and range varies depending on the sample in order to optimize signal. A 90° geometry cell holder is used for solutions, and a 45° geometry film holder is used for thin films.

2.3 Quantum yield

Quantum yield is defined as the number of photons emitted divided by the number of photons absorbed (***equation 2.1***).

$$QY = \frac{\#\ of\ photons\ emmitted}{\#\ of\ photons\ absorbed} \qquad \textbf{(Equation 2.1)}$$

The quantum yield measurement is made on the Jobin Yvon fluorometer by using an integration sphere. Two special cells are used in the integration sphere. A scheme of instrumental setup is shown in ***figure 2.1***. The integration sphere is used to collect "all" the emitted photons for measurement by the detector so that the number of photons emitted can be effectively estimated independent of the geometry of the instrument. To measure the number of photons absorbed by the sample, the monochromator behind the lamp is set at the wavelength of excitation, the spectrum of excitation light when a blank is put into integration sphere is measured as $\boldsymbol{L_a}$, and when the sample is put into integration sphere the spectrum of excitation light is also measured, as $\boldsymbol{L_c}$. The difference between $\boldsymbol{L_a}$ and $\boldsymbol{L_c}$ represents the number of photons that are absorbed. By using the same experimental method but setting the monochromator to scan the whole range of fluorescence, the fluorescence spectra of sample and blank are measured as $\boldsymbol{E_c}$ and $\boldsymbol{E_a}$, respectively. Thus the number of photons emitted is represented by the difference of $\boldsymbol{E_c}$ and $\boldsymbol{E_a}$. The quantum yield is given by ***equation 2.2***:

$$QY = \frac{\#\ of\ photons\ emmitted}{\#\ of\ photons\ absorbed} = \frac{\boldsymbol{E_c - E_a}}{\boldsymbol{L_a - L_c}} \qquad \textbf{(Equation 2.2)}$$

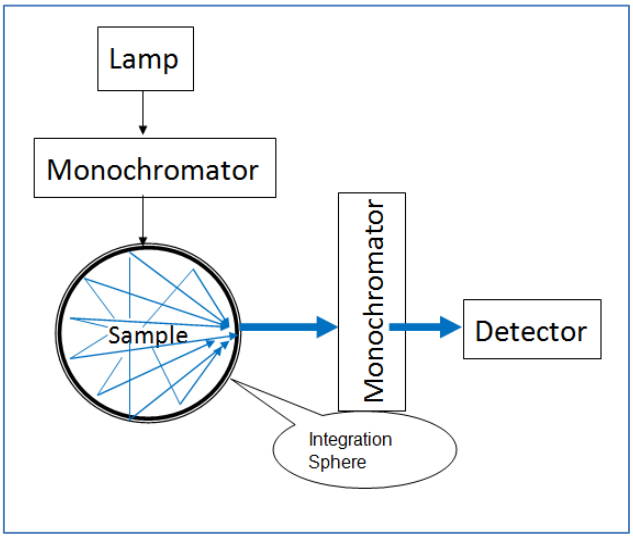

Figure 2.1: Instrumental setup for quantum yield measurement.

It is important to realize that the fluorescence spectrum measurement is not an absolute measurement; the result that comes from the detector is the number of counts per second instead of the number of photons. Although fluorescence spectroscopy is relative, as long as all of the measurements are made on the same fluorometer by using the same parameters, the result of quantum yield which is determined by the quotient of two relative values, will be absolute and accurate. Correction factors are used to take into account the change in sensitivity of the detector as wavelength is changed. A correction factor for the integration sphere can also be used.

2.4 TCSPC

A Time-Correlated Single Photon Counting (TCSPC) system is built to measure excited state lifetime (***figure 2.2***). A Coherent Ti: Sapphire mode locked laser is running to provide excitation pulses at a repetition rate of 76MHz. The laser beam is split into two beams from one by a beam splitter. One laser beam goes to the Fast Trigger Diode and initiates a start signal while another beam goes to excite the sample. The fluorescence of the sample is detected by an Avalanche Photodiode and a stop signal is thus triggered. The time difference between excitation and emission is measured by a Picoharp 300 picosecond timer that acts like a superfast stopwatch (***figure 2.3***). The whole set of instrumentation was built as described in the

accompanying tech note.[30]

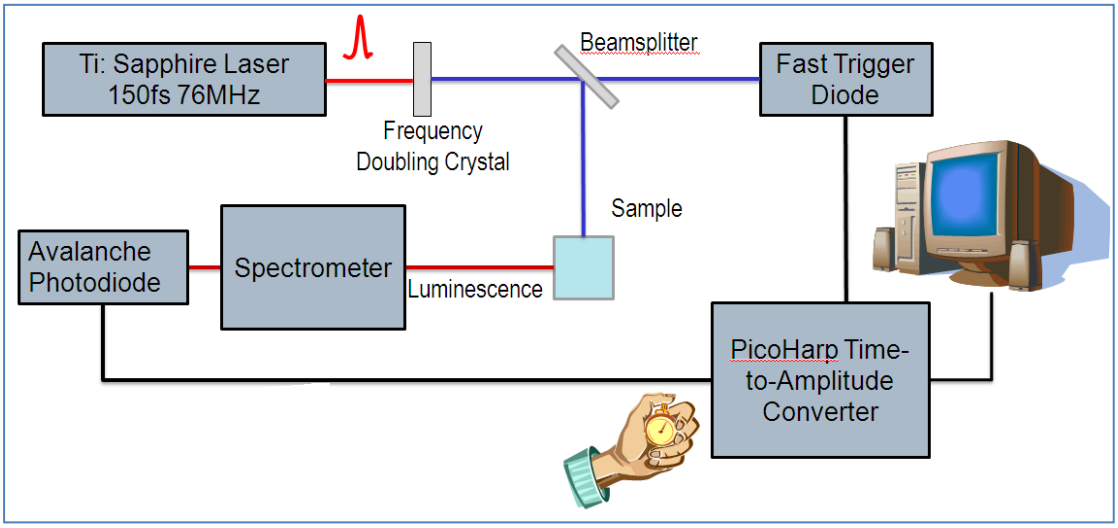

Figure 2.2: A schematic diagram for TCSPC system.

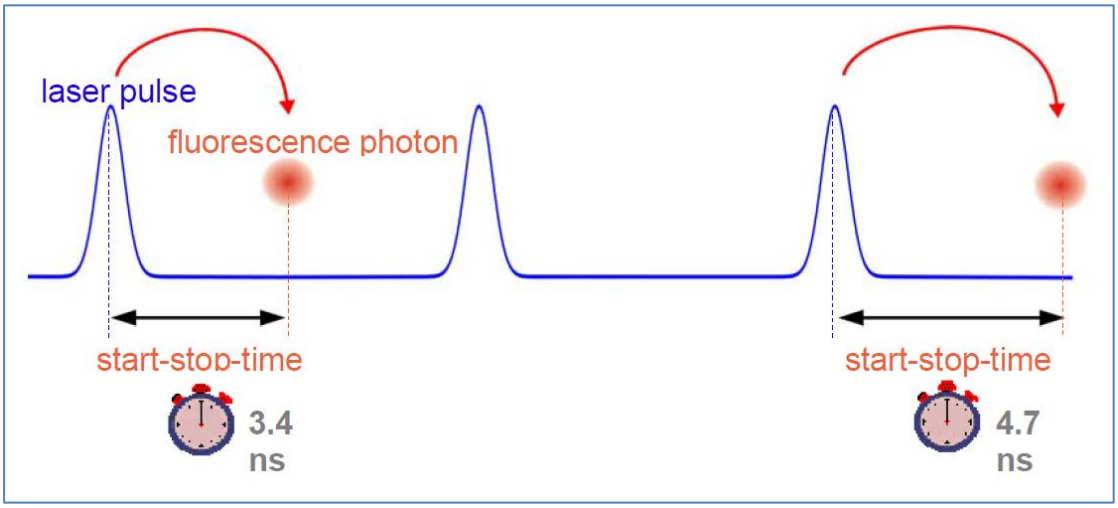

Figure 2.3: The time difference between excitation and emission is measured the Picoharp 300.

Chapter 3

Characterization of squaraines ($DiBSQ(OH)_2$, $DiPSQ(OH)_2$, $DESQ(OH)_2$)

3.1 Experiments:

Photophysical properties of squaraines were determined. The extinction coefficients of squaraines were measured in chloroform. Absorbance spectra, emission spectra and excitation spectra were measured in various solvents with different polarities. All solutions were measured in a quartz cell of path length 1 cm. Absorbance spectra were measured by a Shimadzu High Resolution UV - 2401 spectrophotometer under 0.5nm slit width, medium scan speed. Emission spectra and excitation spectra were measured by Horiba Jobin Yvon FluoroMax-4P spectrofluorimeter under 1.5/1.5nm slit width, 0.5s integration time. A 150 W Xe arc lamp was used as the excitation source. Quantum yields were measured using the Fluorometer and integration sphere as described in the accompanying JY-Horiba application note for the spectrofluorimeter;[31] absorbance of solutions used for quantum yield measurements were kept under 0.1 to minimize reabsorption.

3.2 Data:

$DiBSQ(OH)_2$: The absorbance spectra, fluorescence spectra, and excitation spectra of $DiBSQ(OH)_2$ (***figure 1.10***) in different solvents are presented in ***figure 3.1***. $DiBSQ(OH)_2$ has absorbance maximum at 652nm and emission maximum at 662nm in chloroform. The extinction coefficient of $DiBSQ(OH)_2$ at 650nm in chloroform equals 3.7×10^5 L/(mol*cm) with a 3% error. The λ_{max} of absorbance and the extinction coefficient of $DiBSQ(OH)_2$ are found to be solvent dependent. Detailed data are

presented in ***table 3.1*** and discussed in section 3.3. Before detailed discussion, one feature worth noticing is that when acetonitrile or DMA is the solvent, the shoulder of the excitation spectrum is higher than that seen in absorption. The observed structure is likely associated with vibronic interactions. Higher shoulders in excitation spectra than in absorbance spectra are also found on $DESQ(OH)_2$ and $DiPSQ(OH)_2$ for certain solvents. Differences in absorbance and excitation spectra suggest different quantum yields at the shoulder and the absorption max, worth considering in future work.

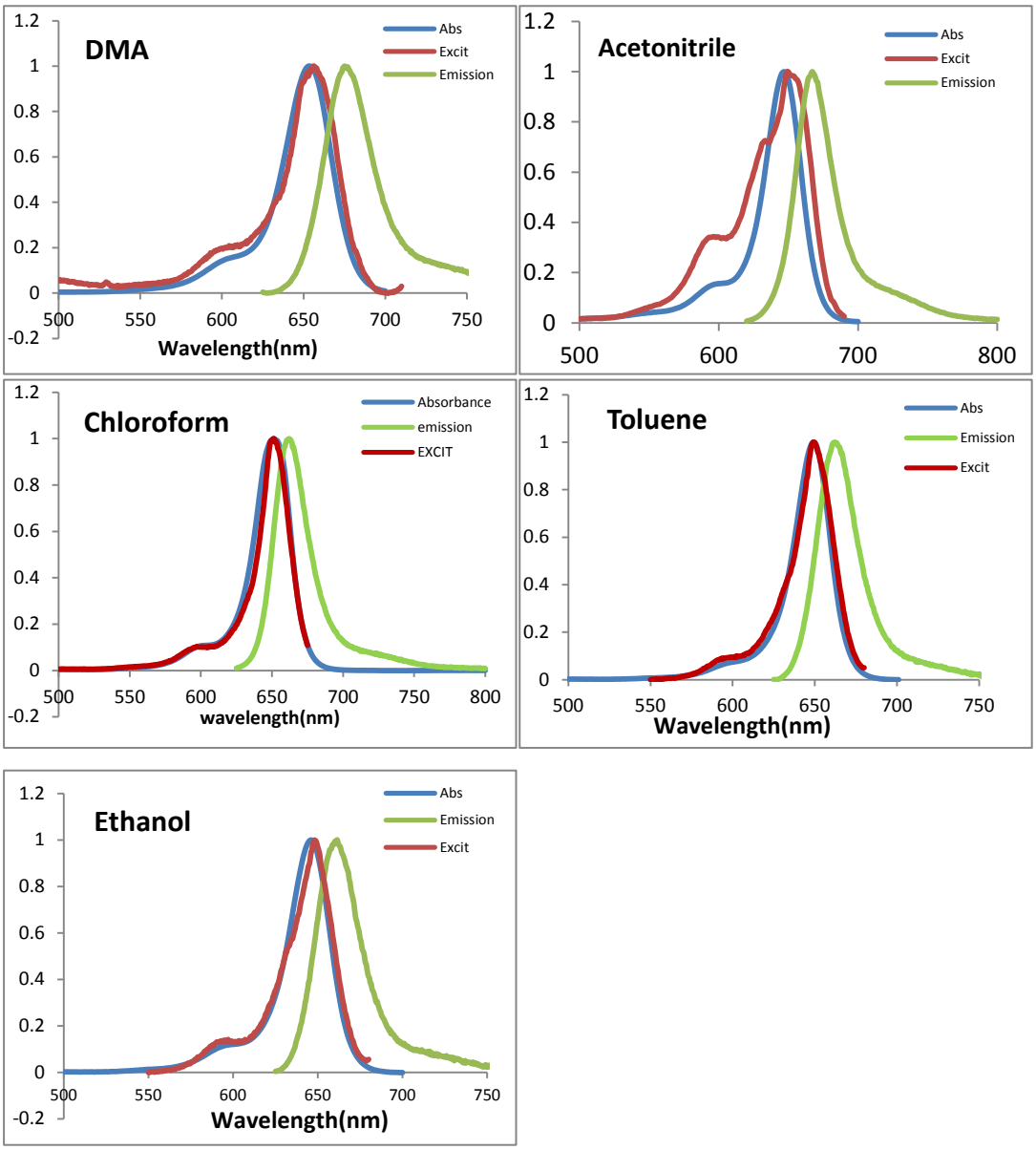

Figure 3.1: Normalized absorbance spectra, fluorescence spectra, and excitation spectra of $DiBSQ(OH)_2$ in DMA, acetonitrile, chloroform, toluene, and ethanol.

DESQ(OH)$_2$: The absorbance spectra, fluorescence spectra, and excitation spectra of DESQ(OH)$_2$ (***figure 1.10***) in different solvents are presented in ***figure 3.2***. DESQ(OH)$_2$ has its absorbance maximum at 644nm and emission maximum at 654nm in chloroform. The extinction coefficient at 650nm in chloroform equals 2.3 x 10^5 L/(mol*cm) with a 3% error. Detailed data are presented in ***table 3.1*** and discussed in section 3.3. When DiBSQ(OH)$_2$ is dissolved in acetonitrile and DMA, the shoulder of each excitation spectrum is higher than of absorption as shown in section 3.2.1. The same phenomenon happens when DESQ(OH)$_2$ is dissolved in ethanol. The same measurement in acetonitrile is still to be made. Usually absorbance spectra and excitation spectra are identical; the difference in height of the shoulders here suggests that squaraine might have more than one form in solution. Law has attributed the shoulder to a distorted form of squaraines.[13] This is an interesting phenomenon worth studying in future research.

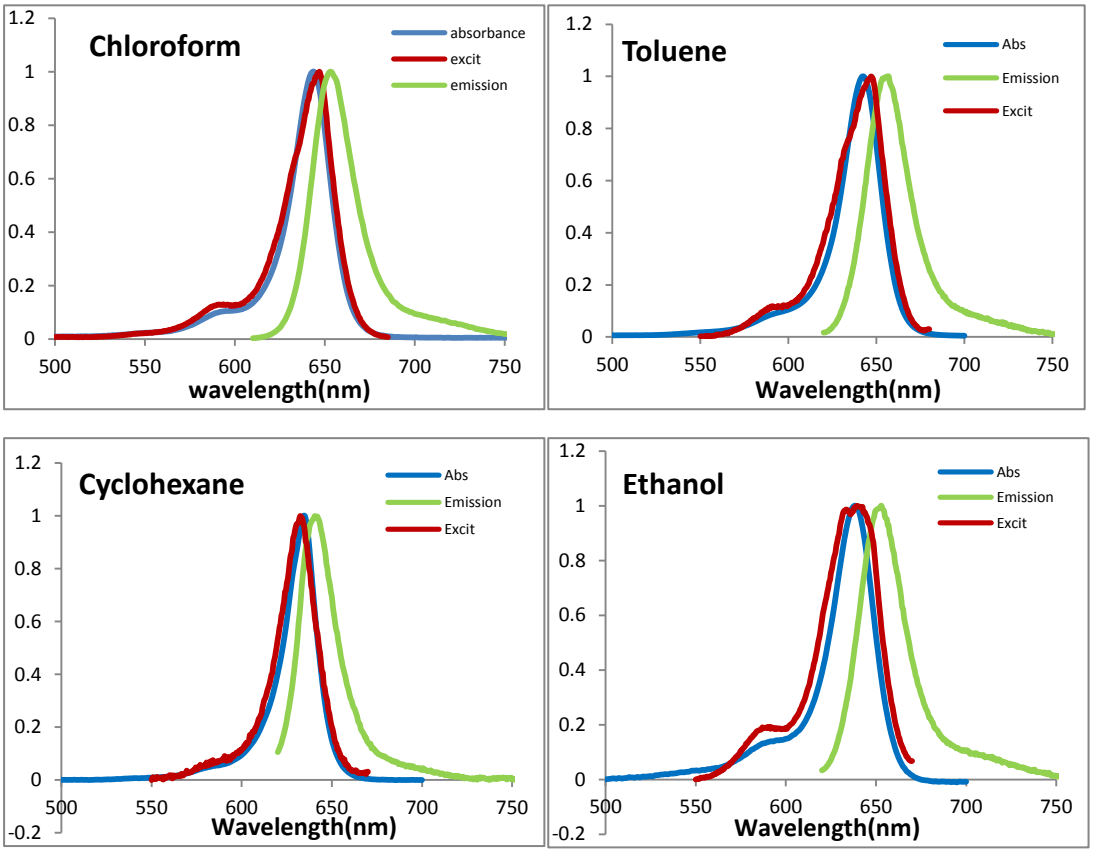

Figure 3.2: Normalized absorbance spectra, fluorescence spectra, and excitation spectra of DESQ(OH)$_2$ in chloroform, toluene, cyclohexane, and ethanol.

DiPSQ(OH)$_2$: The absorbance spectra, fluorescence spectra, and excitation spectra of DiPSQ(OH)$_2$ (***figure 1.10***) in different solvents are presented in ***figure 3.3***. DiPSQ(OH)$_2$ has absorbance maximum at 650nm and emission maximum at 660nm in chloroform. The extinction coefficient at 650nm in Chloroform equals to 2.4 x 10^5 L/(mol*cm) with a 3% error. Detailed data are presented in ***table 3.1*** and discussed in section 3.3. When DiPSQ(OH)$_2$ is dissolved in chloroform, DMA, and in ethanol, the shoulder of excitation spectrum is higher than that of absorption. When chloroform is the solvent, this interesting shoulder is only found on DiPSQ(OH)$_2$.

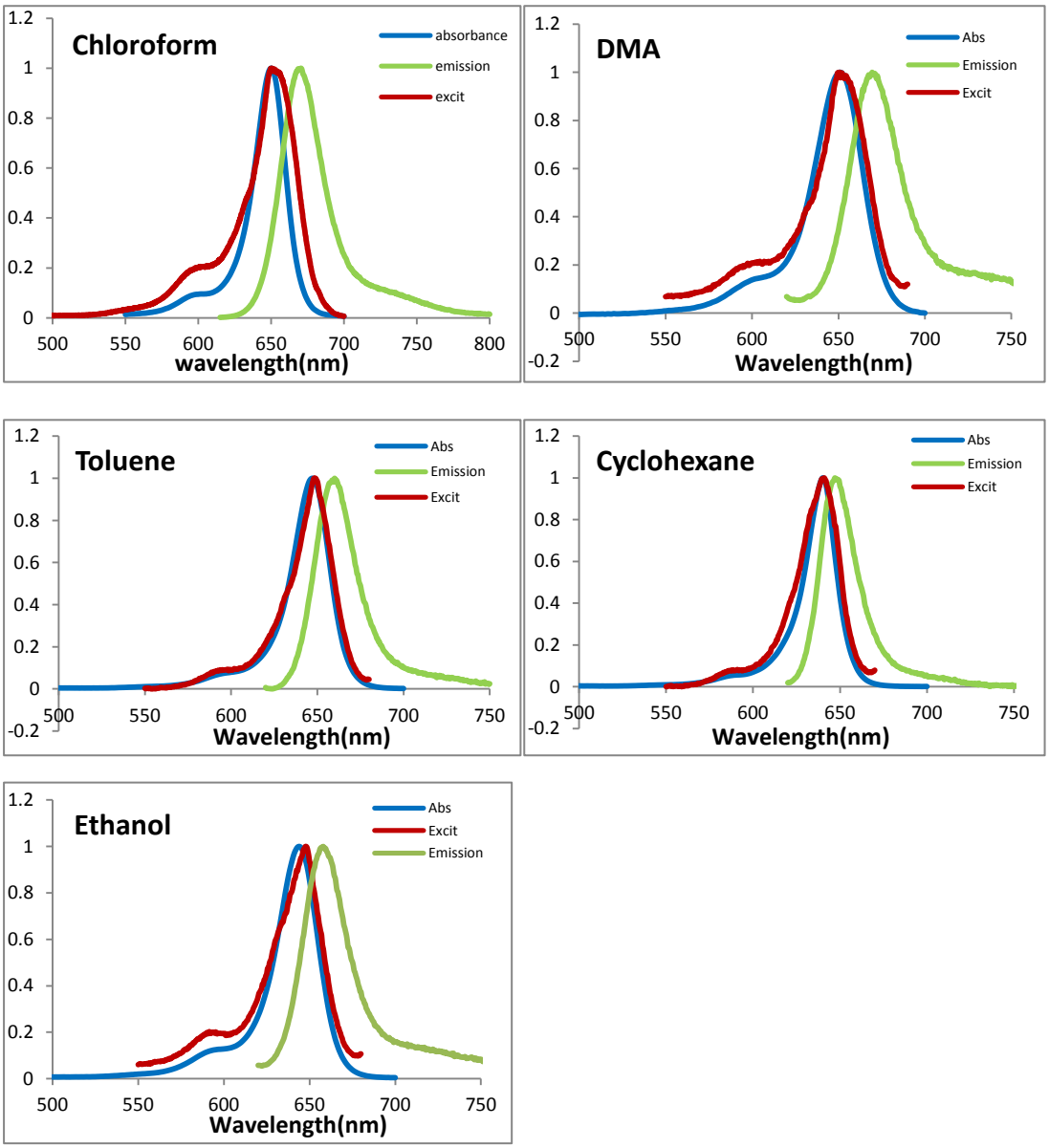

Figure 3.3: Normalized Absorbance spectra, fluorescence spectra, and excitation spectra of DiPSQ(OH)$_2$ in chloroform, DMA, toluene, cyclohexane, and ethanol.

Summary table

Dye	Solvent		Polarity(D)	π*	ε(10^5L/(mol*cm))	Abs max	$FWHM_{Abs}$	Em max	$FWHM_{Em}$	Stokes shift	QY	τ	τ_o
$DIPSQ(OH)_2$	Aprotic	Acetonitrile	3.92	0.75						0	0.25±0.01	2.38	9.52
		DMA	3.72	0.88		651±1	33±2	670±1	34±2	19±2	0.19	1.74	9.16
		Chloroform	1.04	0.76	2.40	650±1	25±2	660±1	34±2	10±2	0.82±0.06	2.4	2.93
		Toluene	0.36	0.54		647±1	25±2	660±1	28±2	13±2	0.26	2.24	8.62
		Cyclohexane	0	0		640±1	20±2	647±1	24±2	7±2	0.24	2.26	9.42
	Protic	Ethanol	1.69	0.54		644±1	28±2	658±1	31±2	14±2	0.28	2.21?	7.89
$DIBSQ(OH)_2$	Aprotic	Acetonitrile	3.92	0.75	2.75	647±1	30±2	667±1	30±2	20±2	0.37±0.08		
		DMA	3.72	0.88	2.01	654±1	34±2	675±1	36±2	21±2	0.34		
		Chloroform	1.04	0.76	3.70	652±1	29±2	662±1	28±2	10±2	0.75±0.04		
		Toluene	0.36	0.54	3.33	649±1	25±2	662±1	29±2	13±2	0.36		
		Cyclohexane	0	0	4.29	642±1	21±2				0.29		
	Protic	Ethanol	1.69	0.54	3.60	646±1	29±2	661±1	32±2	15±2	0.26		
$DESQ(OH)_2$	Aprotic	Acetonitrile	3.92	0.75							0.36±0.02		
		DMA	3.72	0.88		646±1	32±2				0.11		
		Chloroform	1.04	0.76	2.30	644±1	25±2	654±1	28±2	10±2	0.73±0.03		
		Toluene	0.36	0.54		642±1	25±2	657±1	28±2	15±2	0.27		
		Cyclohexane	0	0		635±1	20±2	641±1	24±2	6±2	0.2		
	Protic	Ethanol	1.69	0.54		638±1	27±2	653±1	30±2	15±2	0.24		

Table 3.1: Absorption and fluorescence emission data of squaraines.

3.3 Discussion

a) Absorption:

All three squaraines ($DiBSQ(OH)_2$, $DESQ(OH)_2$, and $DiPSQ(OH)_2$) exhibit intense and sharp absorption bands in the visible region, with the absorption max (λ_{max}) varying from 635nm to 654nm. The λ_{max} of the three squaraines varies depending on the different N-alkyl groups, and different solvents as described below. The absorption and fluorescence emission data of three squaraines are summarized in ***table 3.1***.

i. Effect of N-alkyl substituent: The λ_{max} absorption of squaraines in solution red shifts as the length of the N-alkyl chain increases. As noted in chapter 1, both the ground state and excited state of squaraine are intramolecular CT states[12], and the observed red-shift may be attributed to the stabilization of the CT states by the electron releasing N-alkyl groups. However, this stabilization effect induced by the N-alkyl group might be considered insignificant because (1) alkyl groups are not particularly strong electron donating groups; and (2), as the side group, the alkyl chain is far away from the central chromophore. At the same time we might consider the chromophore to be the donor-acceptor-donor moiety (aniline-4-membered ring-aniline) and therefore the alkyl group can be considered "close enough". Law[32] attributes the main driver of the red-shift accompanying increasing N-alkyl chain length to the formation of a

complex between squaraine and solvent, which interacts more strongly when side chains are longer. This interpretation is confirmed by fluorescence spectra and NMR[33]. Based on this theorem, as the length of N-alkyl chain increase, absorption λ_{max} shift to red, which because the increased CT character shifts the equilibrium to the formation side of the solute-solvent complex. However, while λ_{max} red shifts by 7nm and 5nm, respectively, from DiBSQ(OH)$_2$ (R = C_4H_9) and DiPSQ(OH)$_2$ (R = C_5H_{11}) to DESQ(OH)$_2$ (R = C_2H_5) are observed, there is a blue shift of 2nm from DiBSQ(OH)$_2$ to DiPSQ(OH)$_2$. Also, the red shift is accompanied with a small increase in ε_{max} which is speculated due to the stabilization of charge transfer states induced by electron-releasing N-alkyl groups[9]. Again, while DiBSQ(OH)$_2$ and DiPSQ(OH)$_2$ both have higher ε_{max} than DESQ(OH)$_2$; DiPSQ(OH)$_2$, which has the longest N-alkyl group (***figure 3.4***), and would be expected to have the largest extinction coefficient by this logic, shows a smaller ε_{max} than DiBSQ(OH)$_2$.

DESQ(OH)$_2$:

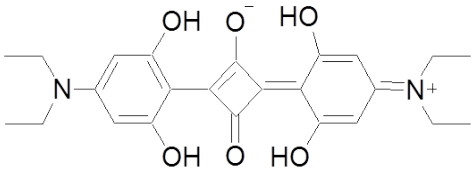

DiBSQ(OH)$_2$:

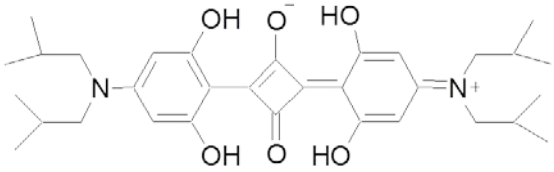

DiPSQ(OH)$_2$:

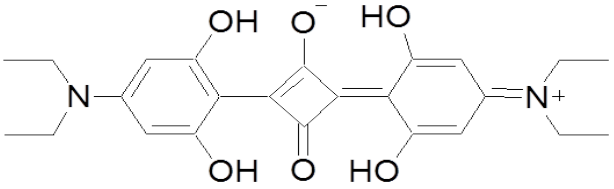

Figure 3.4: Molecular structure of three squaraines.

ii. Characteristic shoulder: A characteristic shoulder in the blue edge of the absorption band is observed on all three squaraines at 595nm (DiBSQ(OH)$_2$), 587nm (DESQ(OH)$_2$), and 595nm (DiPSQ(OH)$_2$) respectively. Interestingly in Law's squaraine review book, such a shoulder is only found on unsymmetrical squaraines and is attributed to vibrational fine structures[9]. In Law's book most of the squaraines are not

C2/C6 OH substituted. Our squaraines have four OH substituents on the C2/C6 positions and because of the strong intramolecular hydrogen bond between the C2/C6 OH substituents and the C—O group, we expect a rigid planar form of squaraine molecule. However, based on Law's assignment of the shoulder to the vibration fine structure of the squaraine molecule, the observed shoulder in the absorbance spectra of our squaraines suggests that despite the presence of strong intramolecular hydrogen bonds, the structure of squaraine is still distorted to some extent.

iii. Solvent effect:

As in ***table 3.1***, small red-shifts are observed for λ_{max} of all three squaraines in polar solvents. The small shifts suggest that there is very little solvent reorganization during the electronic transition. The observation is consistent with literature, and is in agreement with the charge transfer character of squaraine which is similar for both S_0 and S_1 states. This observation also supports the MO calculation results reported by Bigelow and Freund[34], which showed that the S_0 to S_1 transition is localized in the central four-membered ring of squaraine.

A linear relationship between λ_{max} and the Kamlet-Taft solvent parameter π^*[35] is obtained, while the plots using other solvent parameters, such as the dielectric constant, dipole moment, and so forth, are quite scattered. The plot of λ_{max} of all three squaraines as a function of π^* is given in ***figure 3.5***. Linear relationships are obtained in the plot, with the slope of the trend lines being nearly the same for each squaraine. According to Law's review book[9], the solvent effect on λ_{max} results from an equilibrium shift to favor the formation of the complex as π^* increases. Although a systematic and gradual change of λ_{max} has been established for most of the solvents, acetonitrile is an exception.

Along with the red shift of λ_{max}, the absorption peak is slightly broadened in more polar solvents. The FWHM is 10nm more in the polar solvent DMA compared with the non-polar solvent cyclohexane.

The extinction coefficient of squaraine is also found to be solvent sensitive; in

general it decreases as the polarity of solvent increase. This trend is unsurprising since squaraine is characterized by its four-membered ring and phenyl ring intramolecular charge transfer state. Polar solvents distort the planarity of squaraine[36], which reduces the charge transfer state and annuls the extinction coefficient, and as the polarity of solvent increases, squaraine is expected to be twisted more. As a result decreasing extinction coefficients of squaraine are measured.

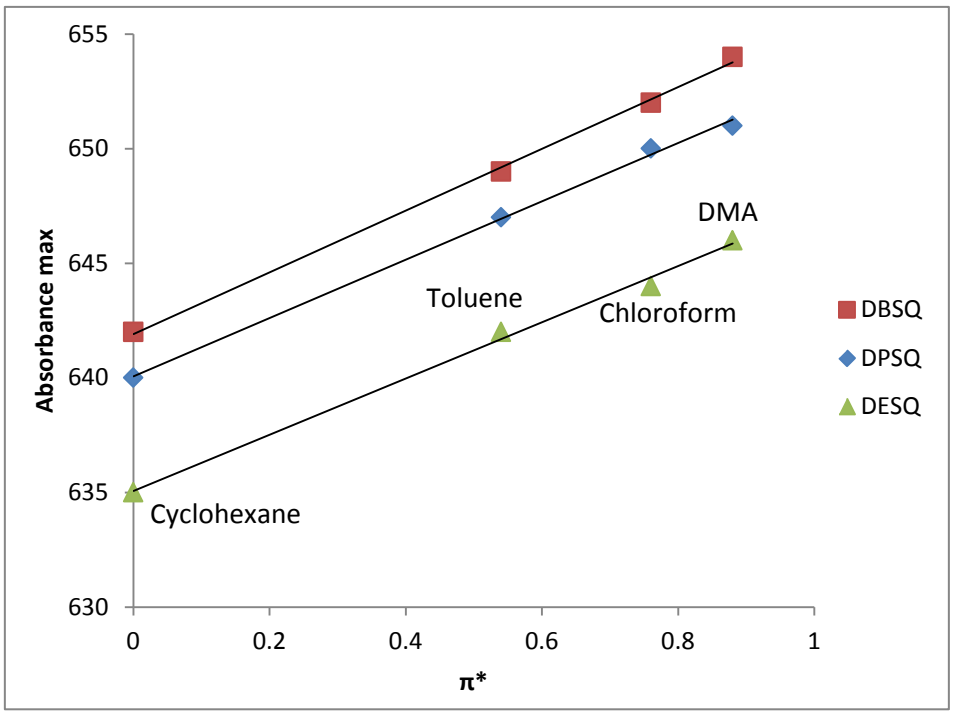

Figure 3.5: Increasing λ_{max} of all three squaraines ($DiBSQ(OH)_2$, $DiPSQ(OH)_2$ and $DESQ(OH)_2$) as a function of π*.

b) Emission

The corrected fluorescence excitation and emission spectra of three squaraines in various solvents are collected in ***figures 3.1~3.3***. The spectral results are summarized in ***table 3.1***. The excitation spectra were found to be more or less identical to the absorption spectra and are independent of the emission wavelength. For each squaraine, only one emission band is observed. However, this one single emission band may in fact be an overlap of two emission bands from two species (squaraine and squaraine-solvent complex)[32]. These two species might be distinguished by fluorescence lifetime studies in the future. The Stokes shifts of fluorescence of

squaraines is small, ranging from 6nm to 21nm depending on the polarity of solvent. Since Stokes shifts are the result of energy losses in the excited state, such small stokes shift may be beneficial for application in OPV cells. The increase of the Stokes shift accompanied by the red shift of absorption and emission spectra induced by polar solvents is relatively small. Although like any typical fluorescence spectra, the emission spectra of the three squaraines are all described well in terms of mirror-image symmetry when compared to the corresponding absorption spectra. The emission peak is slightly wider than the absorption peak, with the FWHM 1nm-4nm larger than the FWHM of absorption peaks. This is consistent with comparison of the FWHM on an energy scale (***table 3.2***), even though each incremental nm in the red has less incremental energy than a corresponding nm in the blue.

Dye	Solvent		$FWHM_{Abs}$ (nm)	$FWHM_{Abs}$ (eV)	$FWHM_{Em}$ (nm)	$FWHM_{Em}$ (eV)
DPSQ	Aprotic	Acetonitrile				
		DMA	33	9.70E-02	34	9.36E-02
		Chloroform	25	7.37E-02	34	9.36E-02
		Toluene	25	7.44E-02	28	7.97E-02
		Cyclohexane	20	6.09E-02	24	7.06E-02
	Protic	Ethanol	28	8.42E-02	31	8.84E-02
DBSQ	Aprotic	Acetonitrile	30	8.92E-02	30	8.32E-02
		DMA	34	9.92E-02	36	9.71E-02
		Chloroform	29	8.52E-02	28	7.90E-02
		Toluene	25	7.39E-02	29	8.17E-02
		Cyclohexane	21	6.34E-02		
	Protic	Ethanol	29	8.65E-02	32	9.08E-02
DESQ	Aprotic	Acetonitrile				
		DMA	32	9.56E-02		
		Chloroform	25	7.53E-02	28	8.11E-02
		Toluene	25	7.55E-02	28	8.06E-02
		Cyclohexane	20	6.20E-02	24	7.22E-02
	Protic	Ethanol	27	8.26E-02	30	8.72E-02

Table 3.2: FWHM of squaraines in wavelength scale (nm) and energy scale (eV).

The increase of the N-alkyl chain length combined with changes in polarity of solvents lead to the red shift and slight broadening of fluorescence because of formation of solute-solvent complexes. Thanks to the rigid planar structure which is reinforced by the strong hydrogen bonds between the oxygen atoms on the central C_4O_2 unit and the C2 hydroxyl substituents on the phenyl rings, the quantum yields of the three squaraines are in the range of 0.73 to 0.82 in chloroform. Such high quantum yields are good for OPV devices. As the N-alkyl chain length increases, the quantum yield increases. This is because the major non-radiative decay process for the excited state of squaraines involves a rotation of the carbon-carbon between the phenyl ring and the

four membered ring; as the size of N,N-dialkylanilino group increases the rate of rotation likely decreases due to increasing steric resistance.

The quantum yield of squaraines is also found to be solvent sensitive (***table 3.1***).

c) Lifetime

The fluorescence decays of DiPSQ(OH)$_2$ in various solvents have been studied and the results are summarized in ***table 3.1***. The fluorescence lifetime decays are mono -exponential. The experimentally measured lifetime τ is relatively insensitive with respect to solvent. The measured lifetime of DiPSQ(OH)$_2$ in chloroform is 2.40±0.1ns, and the values are very close (ranging from 2.21ns to 2.38ns, the only exception is in DMA, which is 1.70ns) in other solvents. It is unusual that the quantum yield decreases from 0.82 to 0.24 while the measured lifetime remains the same. Two possible conclusions could be drawn from this phenomenon. One could hypothesize that a new species which has a longer natural radiative lifetime is formed. Because the natural radiative lifetime τ_o is determined by equation $\tau_o = \frac{\tau}{QY}$, since the quantum yield of squaraine in each solvent is different, the calculated natural radiative lifetime is different as a result (calculated τ_o showed in ***table 3.1***). The natural radiative lifetime τ_o of DiPSQ(OH)$_2$ in chloroform is 2.93ns but in toluene, τ_o is considerably longer at 9.52ns. And since that squaraine-solvent complex has been reported by Law et. al.[33], the prolonged natural radiative lifetime of DiPSQ(OH)$_2$ is assigned to formation of the squaraine-solvent complex.

One might also consider the formation of a dark state (a complex) that absorbs at the same wavelength as the monomer but that does not fluoresce. In this way we would still see the same fluorescence lifetime but it would start to make sense as to why the quantum yield goes down. Of course quantum yield is the number of fluorescence photons divided by the number of absorbed photons. If photons are absorbed by complexes that don't fluoresce then the apparent fluorescence decaytime could stay the same with a drop in quantum yield still being consistent with this data.

3.4 Conclusion:

Photophysical properties (extinction coefficient, absorbance and fluorescence spectra) of three new squaraine dyes were ($DiBSQ(OH)_2$, $DiPSQ(OH)_2$, $DESQ(OH)_2$) characterized.

The λ_{max} of absorbance and the fluorescence peak of the squaraines red shift as the solvent polarity increases. The FWHM of the absorbance peak increases (the peak broadens) as polarity increases.

Chapter 4

Photophysical properties of squaraines in solid states

4.1 Introduction:

So far the photophysical properties of three squaraines have been characterized in various solutions. For the application of OPV devices, we are more interested in the photophysics in the solid state. Photophysical studies on neat films pose a problem in that no fluorescence has been detected on neat films due to strong quenching. Nevertheless, fluorescence study is valuable because it reveals the excited state lifetime which impacts the exciton diffusion length. One can assume the exciton diffusion length is determined by the equation: $D = \tau \times S$, in which D is the exciton diffusion distance, τ is the excited state lifetime, S is the speed of exciton diffusion (the exciton diffusion rate). Higher excited state lifetimes are thus beneficial to the efficiency of OPV devices because they give higher exciton diffusion lengths[8].

In order to investigate the photophysical properties of squaraines in the solid state, we spin-cast squaraines in a solid state solution of Poly methyl methacrylate (PMMA), (***figure 4.1***).

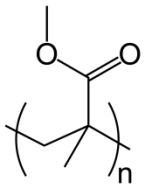

Figure 4.1: Poly methyl methacrylate (PMMA).

PMMA is a transparent thermoplastic which is assumed to not interact with or quench the squaraine. Also PMMA has a good solubility in chloroform, which allows the squaraine and PMMA to disperse evenly in chloroform before spin casting. The concentration of squaraine in solid solution is typically 10^5 to 10^6 times higher than in liquid solution. The process of spin casting neat squaraine films starts with the

chloroform solution of squaraine. As the chloroform quickly evaporates, it is considered that the remaining squaraine molecules are forced closer and closer to each other. With PMMA added, squaraine is locked at the intermediate state from solution to solid. The concentration of squaraine in the solid state is controlled by varying the ratio of squaraine to PMMA, which is assumed to be the same as the ratio in solution. By varying the squaraine/PMMA ratio we attempt to lock the squaraine in certain blend states without the dynamic freedom and motional averaging that typically accompanies liquid solutions in spectroscopic study. We look to obtain valuable information associated with the spin casting process and the morphology of the squaraine thin film. For example, by changing the concentration we hope to investigate the average intermolecular distances as to when the squaraines start to pack to form aggregates. The relative populations of both J- and H-aggregates will thus be investigated.

PMMA films are considered as intermediate states between solution and neat solid phases. The intermolecular distance of the squaraine can be calculated based on the weight ratio of squaraine to PMMA as follows. It is assumed that (1) the density of thin film is equal to that of pure PMMA; (2) adding squaraine does not change the volume of the thin film. Hence, the molarity of squaraine in the thin film (solid solution) can be calculated by:

$$\boldsymbol{M = \frac{mol}{V} = \frac{w\% \times m/FW}{(1-w\%)m/D} = \frac{w\% \times D}{(1-w\%) \times FW}} \qquad \textbf{(Equation 4.1)}$$

In which **M** is the molarity of squaraine in the thin film solution, ***mol*** is the number of moles of squaraine, ***V*** is the volume of thin film, ***w%*** and ***FW*** are the weight ratio and formula weight (molecular mass) of squaraine, respectively, ***m***, which is ultimately canceled out is the mass of the thin film, and ***D*** is the density of PMMA.

With molarity of squaraine thus estimated, the intermolecular distance of squaraine can then be calculated, where ***v*** is the volume taken up by one squaraine in the solid solution and $\boldsymbol{N_A}$ is Avogadro's number:

$$\boldsymbol{l = \sqrt[3]{v} = \sqrt[3]{\frac{V}{N_A MV}} = \sqrt[3]{\frac{1}{N_A M}}} \qquad \textbf{(Equation 4.2)}$$

This approach is based on the assumption that the density of solid solution is

constant and depends solely on PMMA. It is a reasonable approximation when concentration of squaraine is low (weight ratio < 10%), with error estimated to be smaller than 5%. However, when the concentration is high (weigh ratio > 40%), the error based on ***equation 4.2*** is going to be relatively large, ranging from 50% to 100%.

4.2 Experiments and results:

Squaraine thin films were spin-cast at 700 or 1000 RPM when concentration of PMMA was 20 or 56 mg/mL, respectively. Because the concentration of PMMA changes the viscosity of solution which influences the thickness of the films,[37] the spin speed was set lower when the concentration of PMMA was 24mg/mL so as to keep the thickness of films as same as possible. The concentration of PMMA was kept at 56 mg/mL when the weight ratio of squaraine in the solid state is lower than 35%, and 20 mg/mL when weight ratio of squaraine is no less than 35%.

Squaraine and PMMA were dissolved in chloroform, then sonicated at below 40℃ for 10 minutes to make sure the squaraine was fully dissolved. The weight ratio of squaraine to PMMA was varied (so as to change the intermolecular distance of squaraines) in order to investigate the intermolecular interactions and aggregates of squaraines. PCBM was also blended in the film to study the impact of PCBM on morphology and the photophysical properties of films. Absorbance spectra, emission spectra, quantum yields, and fluorescence decay of films were measured.

Films of DiBSQ$(OH)_2$ in PMMA with varied concentration were cast and the absorbance spectra were measured. The weight ratio of DiBSQ$(OH)_2$ to PMMA was varied from 2% to 60%.

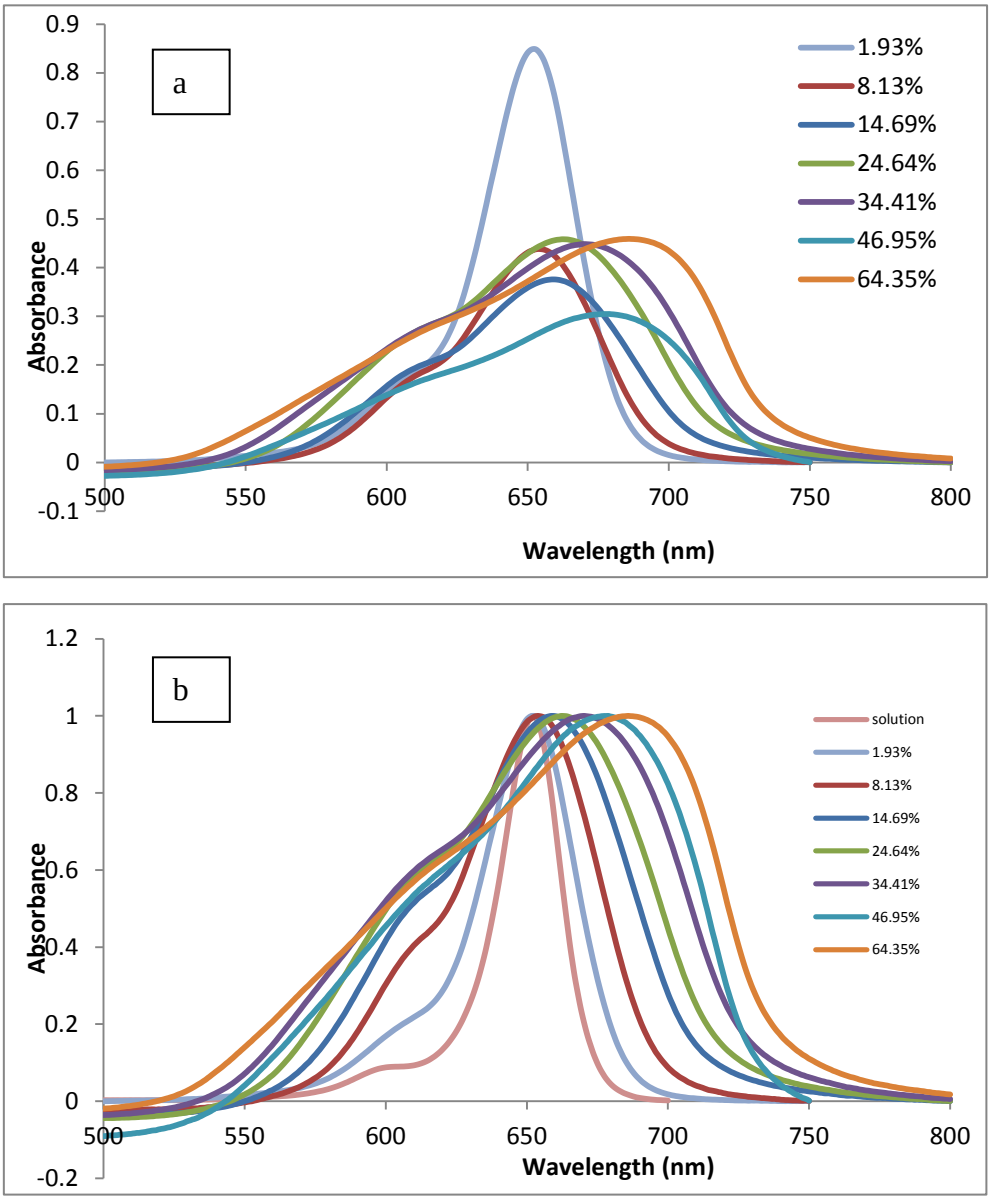

Figure 4.2: The raw absorbance data (a) and the normalized absorbance data (b) of $DiBSQ(OH)_2$ in solid solution as the weight ratio increases; the legend represents the weight ratio of $DiBSQ(OH)_2$ to PMMA used in the solutions used to spin cast the thin film. 56mg /mL and 20mg/mL PMMA stock solutions were used to make all 1.93%-34.41% and both 46.95% - 64.35% samples respectively.

The absorbance peaks broaden and shift gradually as the concentration increases when the weight ratio of $DiBSQ(OH)_2$ is higher than 8%. The question is whether the peaks are gradually shifting because of an unexpected interaction of the squaraine with the PMMA itself, or because a spectrum of aggregates with different absorption wavelengths are starting to form sequentially as the squaraine concentration increases.

Using the same experimental method for making $DiBSQ(OH)_2$ films, $DESQ(OH)_2$ and $DiPSQ(OH)_2$ in PMMA thin films were cast, again with varying weight ratios.

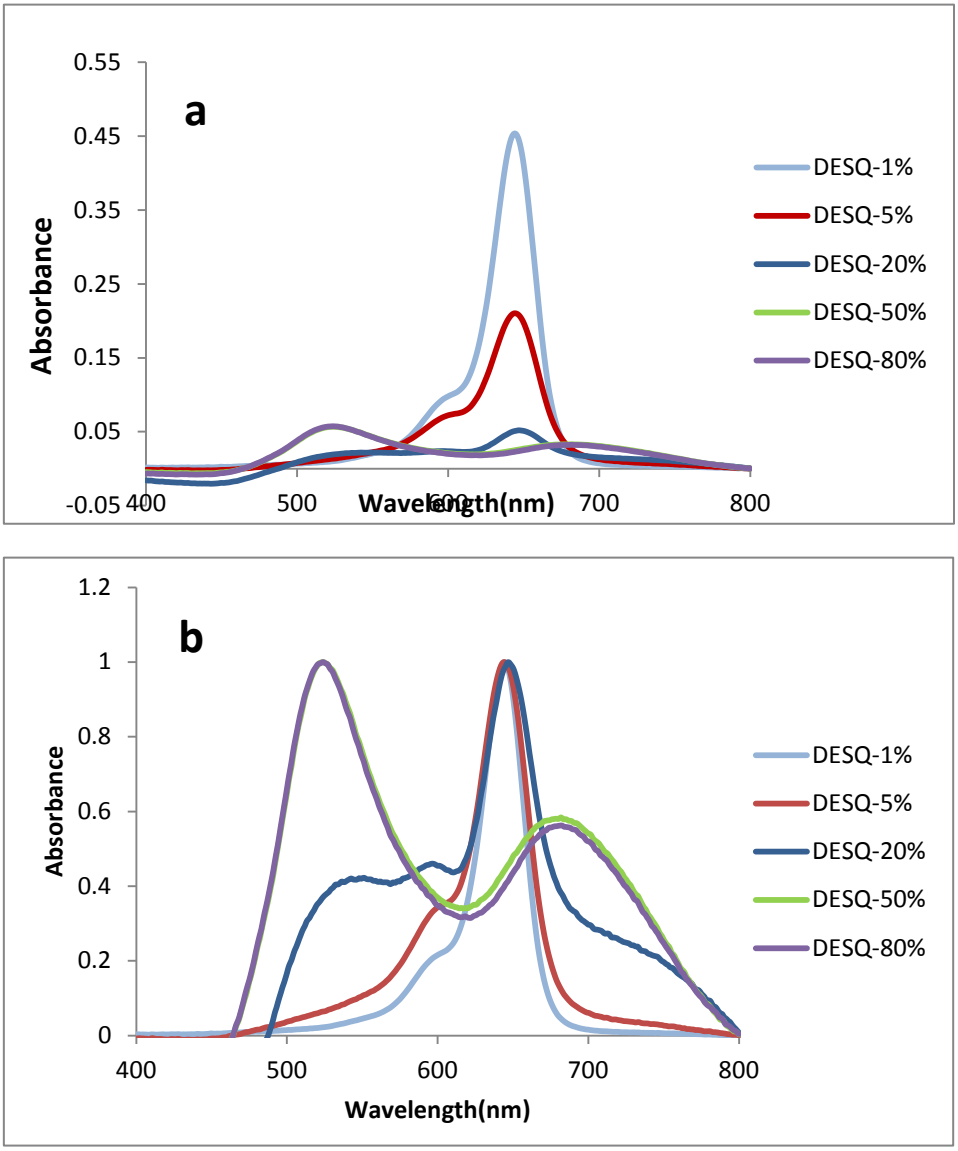

Figure 4.3: The raw absorbance data (a) and the normalized absorbance data (b) of $DESQ(OH)_2$ in solid solution as the weight ratio increases; the legend represents the weight ratio of $DESQ(OH)_2$ to PMMA used in the solutions used to spin cast the thin film. 56mg /mL and 20mg/mL PMMA stock solutions were used to make all 1-20% and both 50% - 80% samples respectively.

Peak broadening happens when the weight ratio of $DESQ(OH)_2$ is higher than 5%. Furthermore a slight red shift of the assigned monomer peak from 644nm to 647nm occurs when the weight ratio of $DESQ(OH)_2$ increases from 5% to 20%. An H-aggregate peak (λ_{max} = 524nm) is assigned when the weight ratio of $DESQ(OH)_2$ is above 20%. By comparison there is no gradual shifting associated with these spectral changes, in contrast to what was observed for $DiBSQ(OH)_2$. This led to an argument about the assignment of the peak at 682nm. It might be a red-shifted monomer peak since it only mildly red shifts from 647nm at a weight ratio of 20% to 682nm at 50%.

However, it appears more likely to be a J-aggregate peak when weight ratio of $DESQ(OH)_2$ increases from 50% to 80% and there is no further red shift.

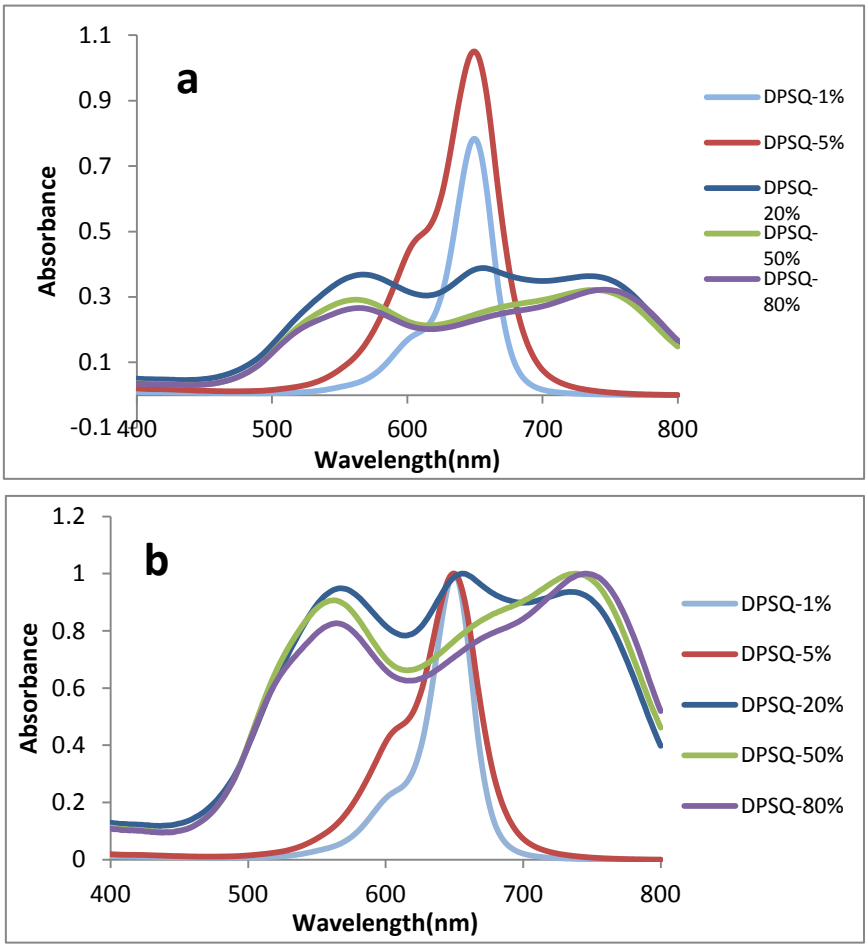

Figure 4.4: The raw absorbance data (a) and the normalized absorbance data (b) of $DiPSQ(OH)_2$ in solid solution as the weight ratio increases; the legend represents the weight ratio of $DiPSQ(OH)_2$ to PMMA used in the solutions used to spin cast the thin film.

With $DiPSQ(OH)_2$, peak broadening happens when the weight ratio of $DiPSQ(OH)_2$ is higher than 5% and again a very slight red shift of the monomer peak from 650nm to 656nm happens when the weight ratio of $DiPSQ(OH)_2$ increases from 5% to 20%. An H-aggregate peak (λ_{max} = 524nm) and a J-aggregate peak (λ_{max} = 745nm) are assigned. Once again there is no gradual shift as the spectrum changes. There appears to be an abrupt increase in the population of H- and J-aggregates, in contrast to the case with $DiBSQ(OH)_2$ where only a gradual shift is apparent. As the study on solid solutions revealed, the aggregation properties of these three squaraines are found out to be more complicated than our expectation. Future studies are needed to de-convolute the aggregation spectra of squaraines. If possible I would recommend a further study by

Langmuir-Blodgett (LB) films, which could give a single phase for aggregation.[38]

4.3 Discussion:

The three squaraines show the same character in absorption spectra in PMMA film only when the concentration of squaraine is small, i.e. only when the weight ratio of squaraine is smaller than 5%. An obvious splitting and broadening of the absorbance band is observed when squaraine weight ratios exceed the threshold of 10%. Interestingly, although the only difference on structure of three squaraines is one or two carbon atoms on the N-alkyl side group, and in solution they all exhibit the similar optical properties in every aspect, their absorption spectra in solid solutions and thin films are very different and distinct from each other.

The absorption peak of $DiPSQ(OH)_2$ in the solid state is split into three distinct peaks, one blue-shifted peak centered at 556nm, one significantly red-shifted peak, centered at 740nm, and one slightly red-shifted peak within 10nm of the corresponding solution peak. The absorption peak of $DESQ(OH)_2$ in the solid state is split into two distinct peaks, one blue-shifted peak centered at 520nm, and one red-shifted peak centered at 678nm (about a 30nm shift from the corresponding monomer peak, in solution). It is believed that the different splitting of the absorption peaks is due to the different ways the squaraine molecules pack. The blue-shifted peaks of $DiPSQ(OH)_2$ and $DESQ(OH)_2$ are both assigned to H-aggregates, while the significantly red-shifted peak of $DiPSQ(OH)_2$ is assigned to a J-aggregate.

a) $DiBSQ(OH)_2$ PMMA films

Unlike $DiPSQ(OH)_2$ and $DESQ(OH)_2$ which show distinct blue-shifted and red-shifted absorption peaks, only one broadened and red-shifted peak (from 652nm to 685nm) is observed for $DiBSQ(OH)_2$ PMMA films. There is an argument about the slightly red-shifted peak of $DiBSQ(OH)_2$, because there are no two peaks that are seen

to be distinctly and conclusively split; it is hard to decide whether the red-shift is owing to an actual J-aggregate species which overlaps the absorption peak of the monomer or whether the single monomer has simply red shifted and broadened because of the PMMA environmental conditions. To figure out which assumption is right, the following experiment is designed.

Four DiBSQ(OH)$_2$-PMMA films are spin cast. The concentration of PMMA is fixed while the concentration of DiBSQ(OH)$_2$ is varied. The speed of spin casting and the volume of the solution dropped on glass are kept the same for all films. Because the thickness of film is controlled mostly by the concentration of PMMA, four thin films with the same thickness but varied concentration of DiBSQ(OH)$_2$ are then produced. The absorption spectra of the films are measured and presented in ***figure 4.5a***. A set of normalized absorption spectra is also presented in ***figure 4.5b***, and is compared with the normalized absorbance spectra of DiBSQ(OH)$_2$-PMMA films, presented before in ***figure 4.2***. The two graphs are very comparable, giving the same trend of gradual broadening and red-shifting. In both ***figure 4.5b*** and ***figure 4.2***, the normalized absorbance spectra of DiBSQ(OH)$_2$-PMMA films have broadened with FWHM increasing from 0.11eV to 0.34eV and the λ_{max} red-shifting from 652nm to 685nm, as the weight ratio of DiBSQ(OH)$_2$ is increased from less than 10% to more than 60%.

With the thickness of PMMA thin films fixed, the relative absorbance extinction coefficient of DiBSQ(OH)$_2$ under different weight ratios can be measured. According to the aggregate experiments of squaraines in solution in chapter 6, the extinction coefficient of DiPSQ(OH)$_2$ J-aggregate at 760nm is only 0.48×10^5 L/(mol*cm), which is about five times less than the extinction coefficient of the monomer at 650nm (2.4×10^5 L/(mol*cm)). The comparison of extinction coefficients between aggregate and monomer is helpful to understand the absorbance peak of DiBSQ(OH)$_2$ at 682nm, which could either be a J-aggregate peak or a red-shifted monomer peak. If we assume that it is a J-aggregate for DiBSQ(OH)$_2$ which has similar properties as DiPSQ(OH)$_2$, then the extinction coefficient of DiBSQ(OH)$_2$ J-aggregate would likely also be about

five times less than that of the monomer. If the aggregate is dominant in the high weight ratio samples and this is the reason for the red shift, then the relative extinction coefficient at absorption λ_{max} is expected to be much lower than for a film with only monomer present, that is a film without a significant red-shift. In other words since the aggregate is speculated to have a low extinction coefficient then we would expect to see a very low absorbance in a PMMA film with the highest concentration of $DiBSQ(OH)_2$.

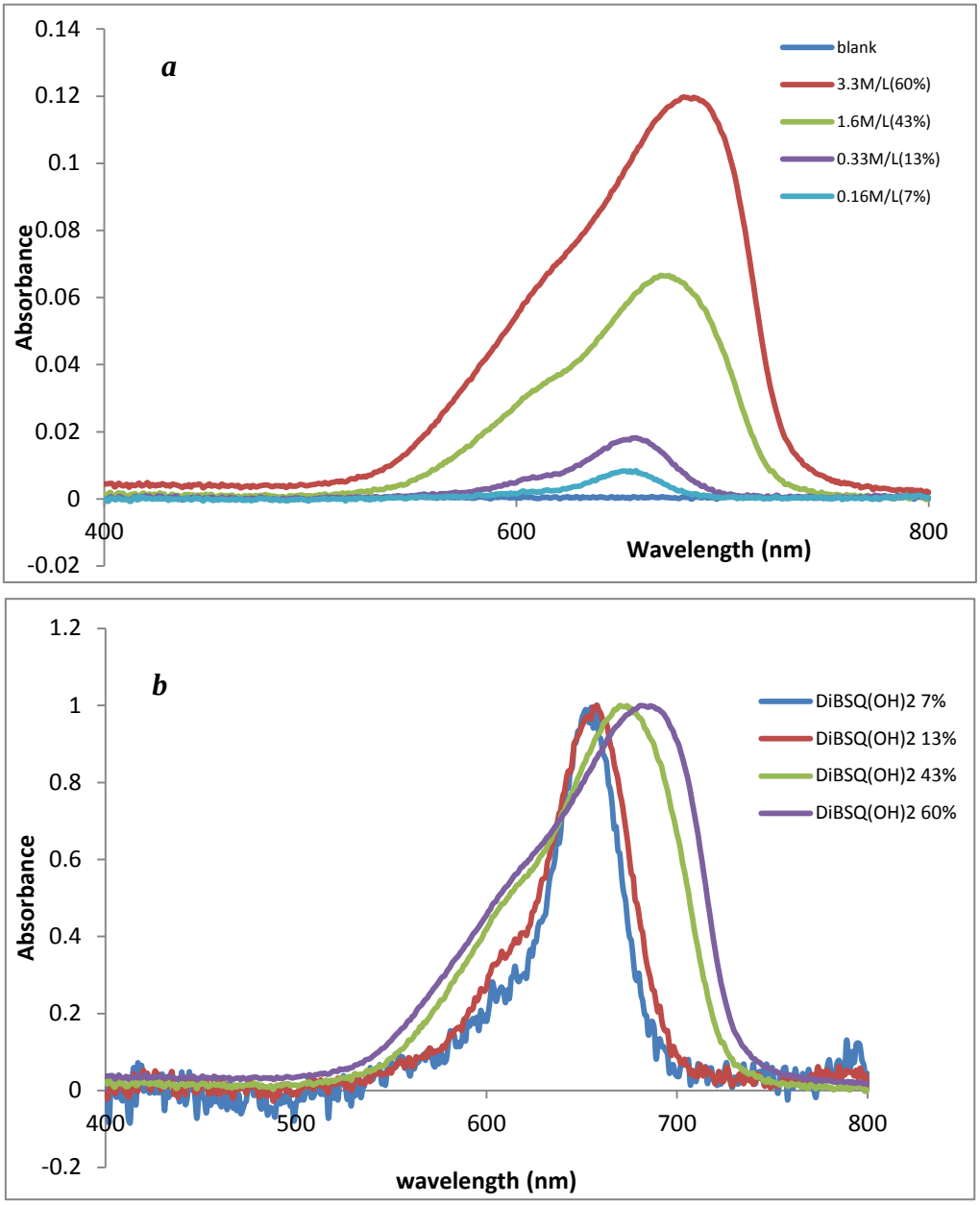

Figure 4.5: (***a***) Absorbance spectra of $DiBSQ(OH)_2$-PMMA films. Concentrations of $DiBSQ(OH)_2$ are varied while the thickness of films are fixed. (***b***) Normalized absorbance spectra of $DiBSQ(OH)_2$-PMMA films in ***a***.

W%	mol/L	Abs at λ_{max}	$\varepsilon * l$ (L/mol)
60%	3.25	0.11974±3%	3.68×10^{-2}±50%
43%	1.63	0.06662±3%	4.10×10^{-2}±40%
13%	0.33	0.01822±3%	5.60×10^{-2}±20%
7%	0.16	0.00842±3%	5.18×10^{-2}±10%

Table 4.1: Comparison of extinction coefficient of $DiBSQ(OH)_2$ in PMMA film at monomer peak (650nm, low concentration) and suspected aggregate (or red-shifted monomer) peak at 682nm (high concentration). Absorbance was measured with good accuracy, with less than ±3% errors. Molarity and extinction coefficient on the other hand, wasn't able to be determined accurately, the error for these two value could up to ±50%.

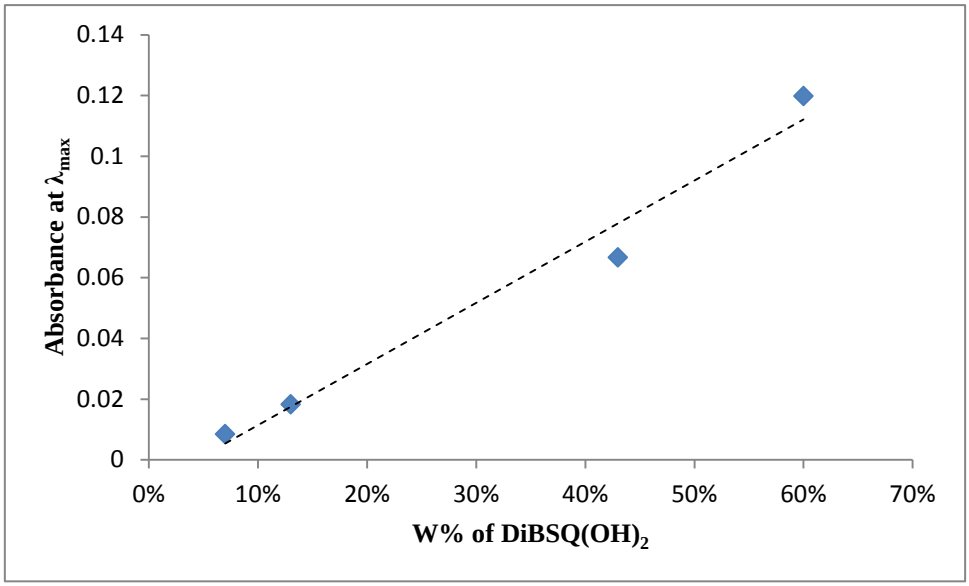

Figure 4.6: Absorbance at λ_{max} versus weight ratio of $DiBSQ(OH)_2$ in PMMA films when thicknesses are controlled to be the same by keeping a fixed concentration of PMMA.

By Beer's Law, extinction coefficient can be found by equation: $\boldsymbol{\varepsilon = A/cl}$. Since the thickness is hard to be measured for thin films, the absolute extinction coefficient ε can't be determined. Nevertheless, as the thickness is kept the same for all the thin films, a pseudo extinction coefficient ($\boldsymbol{\varepsilon l = A/c}$) can be determined and still comparable. As ***table 4.1*** shows, the "extinction coefficient" of $DiBSQ(OH)_2$ in PMMA film is determined to be 5.18×10^{-2}L/mol for the monomer peak (650nm) and 3.68×10^{-2}L/mol for the suspected aggregate (or red-shifted monomer) peak at 682nm. ***Figure 4.6*** also shows when the thickness of thin films is fixed, the absorbance increases linearly as a

function of weight ratio of DiBSQ(OH)$_2$. This is not expected given the hypothesis that the extinction coefficient of the aggregate is about five times less than that of the monomer. As described in chapter 3 (***table 3.1***), the absorbance λ_{max} of DiBSQ(OH)$_2$ red-shifts from 642nm to 654nm when the solvent changes from a nonpolar solvent (cyclohexane) to a polar solvent (DMA). Law has also proved that the absorbance λ_{max} of squaraine can be red-shifted under a polar environment[32]. Squaraines themselves are polar molecules and when more squaraines are introduced to the PMMA film, they replace some of the surrounding PMMA material for each absorbing squaraine molecule. For this reason, I hypothesize that a polar environment is thus created, which results in the red-shifted and broadened absorption peak in DiBSQ(OH)$_2$ films.

For the same reason I hypothesize that the red-shifted absorption peak at 682nm (***figure 4.3***) in the DESQ(OH)$_2$ PMMA solid solution film is assigned to a monomer. In DiPSQ(OH)2 films, the red-shifted monomer peak is likely present but overlaps with the J-aggregate peak. But since this hypothesis need to be proved by further experiment, the following discussion will still using the more general accepted model of aggregation.

The following hypothesis remains: the photophysical properties of the three squaraines in solution are similar because the chromophores share similar electronic properties and electronic structures. One might expect that similar aggregate patterns would be reflected in similar thin film absorption properties. However, the absorption spectra of these three squaraines in thin film are so different to each other, which suggest that they pack in very different ways.

b) DESQ(OH)$_2$ and DiPSQ(OH)$_2$ PMMA films

Although the monomer peaks in the PMMA films of the three squaraines are hard to assign, the aggregate peaks are relatively clear due to the distinct splitting of the absorption band. Giving the red/blue shift of the absorbance peak, I hypothesize the blue and shifted absorbance band as H- and J-aggregates, respectively, for DiPSQ(OH)$_2$,

and the blue shifted absorbance band as H-aggregates for $DESQ(OH)_2$. It is seen that aggregates are not detected until the weight ratio, i.e. the concentration of $DiPSQ(OH)_2$ or $DESQ(OH)_2$, exceeds a certain threshold ratio.

The absorbance at the λ_{max} of the aggregate band in the normalized absorption spectra (***figure 4.2-4.4***) for three squaraines as a function of average intermolecular distance is plotted in ***figure 4.7*** and ***figure 4.8***.

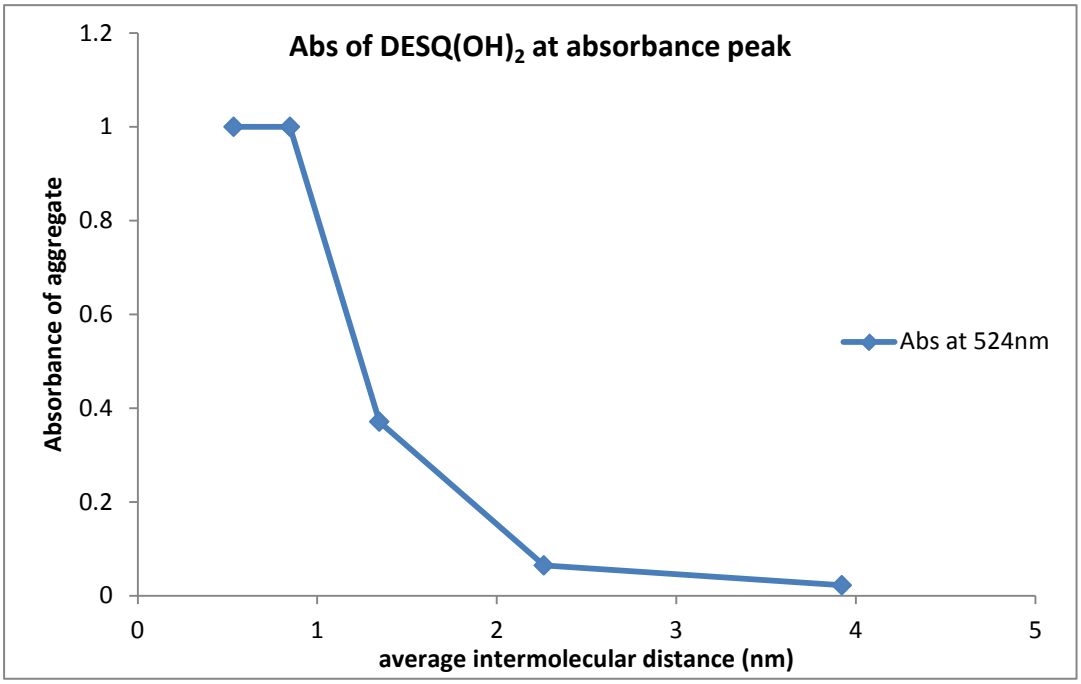

Figure 4.7: Absorbance at the λ_{max} of the aggregate band in the normalized absorption spectra versus the average intermolecular distance.

As the plot shows, the H-aggregate of $DESQ(OH)_2$ is not present until the average intermolecular distance is less than 2nm, based upon the described approach for determining average internuclear separation. The small incremental increase in absorbance before this apparent threshold is due to the broadening of the monomer peak, although the mechanisms for broadening should be considered for completion. Absorbance of the H-aggregate increases significantly when the average intermolecular distance decreases from 2nm to 0.8nm, and then keeps constant as the average intermolecular distance decreases further.

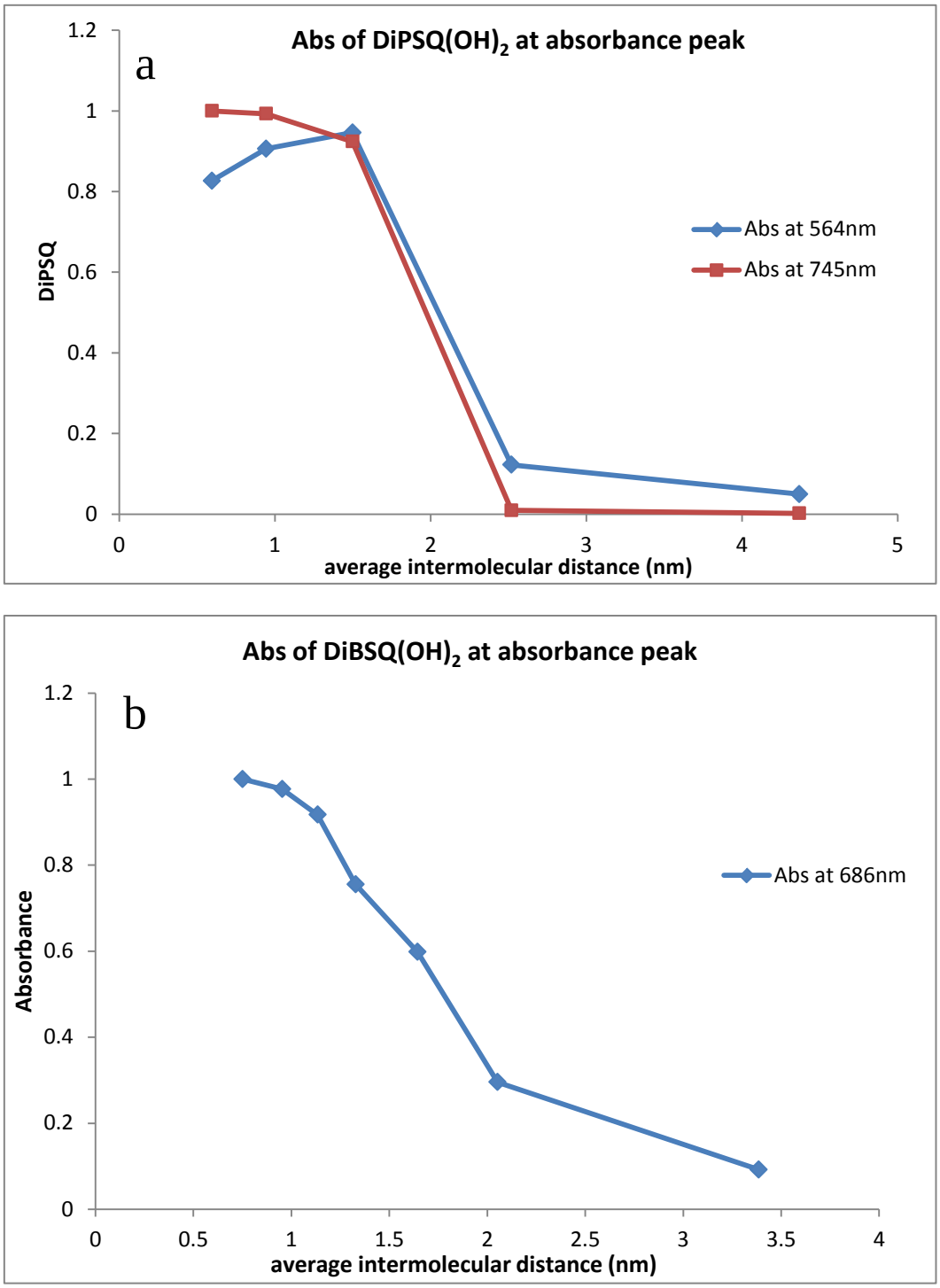

Figure 4.8: Absorbance of (**a**) $DiPSQ(OH)_2$ and (**b**) $DiBSQ(SQ)_2$ at the λ_{max} of the aggregate band in the normalized absorption spectra versus the average intermolecular distance.

A similar plot is shown for $DiPSQ(OH)_2$ in ***figure 4.8a***, a plot for $DiBSQ(OH)_2$ (***figure 4.8b***) is also shown for comparison. Although both types of aggregate are observed on $DiPSQ(OH)_2$, the same trend is found. No aggregates are detected before the average intermolecular distance decreases to an apparent threshold of ~2.5nm and

then the absorbance of both H- and J-aggregates dramatically increases from 2.5nm to 1.5nm, and only shows minor changes for further increasing concentration.

c) De-convolute aggregation by comparing FWHM

Although it is hard to generalize the aggregation properties of these three squaraines by looking through the λ_{max} of aggregate peaks, there is a better trend if we look at the width of the absorption band (which is featured by FWHM).

The FWHM of the aggregate band in the normalized absorption spectra as a function of average intermolecular distance is plotted in ***figure 4.9***. The FWHM increases as average intermolecular distance decreases for all three squaraines generally, indicating an increasing extent of aggregation as squaraines concentrating in PMMA films.

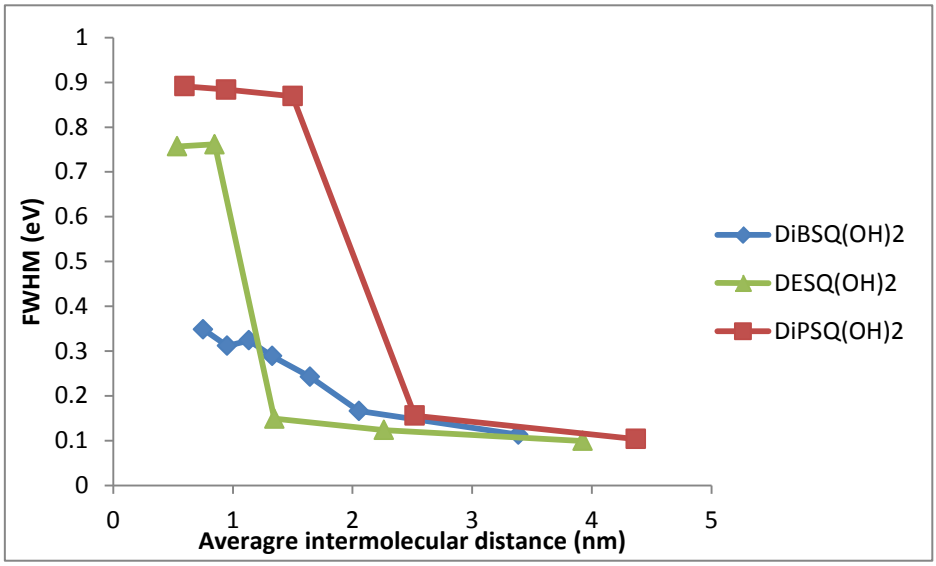

Figure 4.9: The FWHM of the aggregate band in the normalized absorption spectra as a function of average intermolecular distance for DiBSQ(OH)$_2$, DESQ(OH)$_2$, and DiPSQ(OH)$_2$.

We expect the steric hindrance induced by the N-Alkyl group to increase as the length of the alkyl chain increases.[13] Consequently we expect the additional steric hindrance will restrict formation of aggregate and reduce the splitting of absorption spectrum. As the support of this hypothesis, we have observed that in thin films of DiBSQ(OH)$_2$ the splitting of the absorption spectrum is significantly less pronounced than DESQ(OH)$_2$, with the FWHM barely increased from 0.11eV to 0.35eV (***figure***

4.9). The relative height of the H-aggregate peak is less than the J-aggregate in the aggregate spectrum of $DiBSQ(OH)_2$. Although it is hard to say less H-aggregate is formed in $DiBSQ(OH)_2$ because we don't know what exactly the extinction coefficients are, this interpretation is consistent with the exciton model of aggregation. According to the exciton model, the H-aggregate is due to a dipole-dipole interaction requiring a rigid "face-to-face" geometry (***figure 1.8***), while the J-aggregate can be resulted by intermolecular CT which allows a more flexible "head-to-tail" geometry (***figure 1.8***). We are not surprised to see the J-aggregate to be preferred as the length of the N-Alkyl chain increases, since less steric hindrance[39] is expected in the "head-to-tail" geometry in which side groups are staggered, suggesting that H-aggregate is more sensitive to the additional steric hindrance. Unlike $DESQ(OH)_2$ which shows a sharp discrete increasement on FWHM accompanied with the distinct split of absorption bands, $DiBSQ(OH)_2$ gradually broadens the absorption peak as weight ratio is increased while the absorption spectrum appears to remain a single peak; no obvious distinct peak splitting is observed. We still can attribute it to the overlap of aggregate peaks and monomer peaks, which has been reported by Law et. al.[13].

A general diagram for the process of the formation of aggregates based on the squaraine side group is then proposed (***figure 4.10***) and may be used as a testable hypothesis for future ongoing experiments with PMMA solid solutions. As the length of side groups increases, the exciton splitting which is represented by FWHM of the absorbance band is expected to be smaller. Distribution and r_{mid} value, on the other hand, are expected to be bigger.

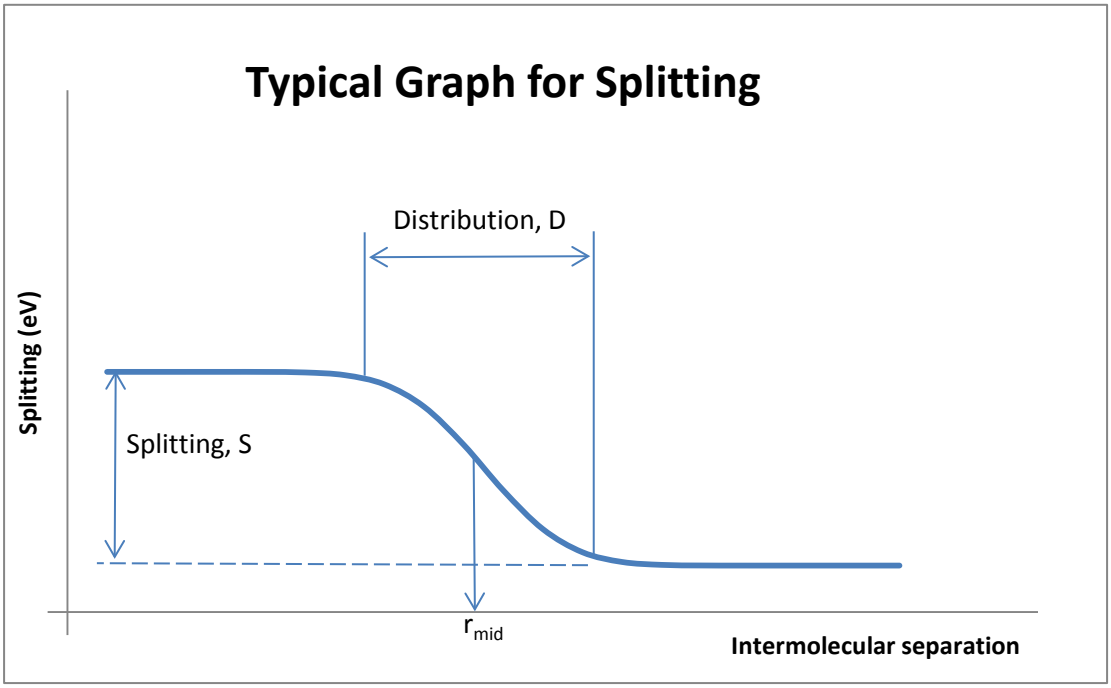

Figure 4.10: a general diagram proposed for exciton splitting in aggregation, smaller splitting is expected for larger sidegroups.

However, as we keep increasing the alkyl chain length further, we unexpectedly observed a very sharp increase of FWHM on $DiPSQ(OH)_2$ (***figure 4.9***), where the H-aggregate and J-aggregate bands are distinctly split. The 0.89eV FWHM of $DiPSQ(OH)_2$ at an average intermolecular distance of 0.59nm is even bigger than $DESQ(OH)_2$. This unexpected sharp splitting suggests that the "iso" N-Alkyl chain may induce other interactions apart from steric hindrance. My interpretation is the alkyl chains entangle and enhances aggregate if the length is too long. This however is speculative.

4.4 Conclusion:

The absorption spectra of three squaraines in PMMA films have been studied. For each squaraine in a PMMA solid solution a different absorption band is observed, suggesting that the influence of the side group on the molecular packing is important. It may also be that the squaraine complexes differently with the PMMA molecules as the side group is changed, but this explanation seems more complicated, especially given

that the absorbance spectra of the solid solutions start to approach the absorbance spectra of the films, in general. In summary, $DESQ(OH)_2$ forms H-aggregates only, $DiBSQ(OH)_2$ does not appear to aggregate, and $DiPSQ(OH)_2$ forms both H-aggregate and J-aggregate at the same time. Still, further works are needed to test and confirm the hypothesis and explanations.

For future investigation of aggregate properties of squaraines, similar PMMA films can be annealed such that phase separation starts to take place and aggregation would likely occur at lower concentrations. In this way, by taking a relatively dilute PMMA/Squaraine film, where there are no aggregates present in the pristine film, we can look to see if aggregates form when we heat the film up to just below the polymer melting point. In this case we would not expect the thickness of the film to change but we would hope to see a spectroscopic difference that would likely only be explainable by the aggregation through phase separation. This would help us with clearer assignments of the peaks. We can also study the change in fluorescence decay time and quantum yield as we encourage this aggregation. This experiment is helpful to de-convolute the spectra of aggregate-monomer mixtures, especially if aggregate peak and monomer peak are overlapped.

Chapter 5

The Impact of Aggregation on Fluorescence

5.1 Introduction

The process of exciton diffusion is crucial to the efficiency of OPV devices. The essence of exciton diffusion is energy transfer, that is to say the motion of electronic excited states between molecules. Two types of intermolecular interactions could enhance transfer of excitation energy from donor to acceptor in a bimolecular process (***figure 5.1***): columbic energy transfer (Forster energy transfer) and electron exchange transfer (Dexter energy transfer). Förster energy transfer is caused by long range (up to 10nm) dipole-dipole interactions while Dexter energy transfer requires that donor and acceptor (D* and A) stick with each other (0.6~2nm). When donor and acceptor are both squaraine molecules, the exciton may diffuse either by repeating the process of Förster energy transfer or Dexter energy transfer. Förster energy transfer undergoes a mechanism of dipole-dipole coupling and can occur in a range considerably exceeding the range of van der Waals force.

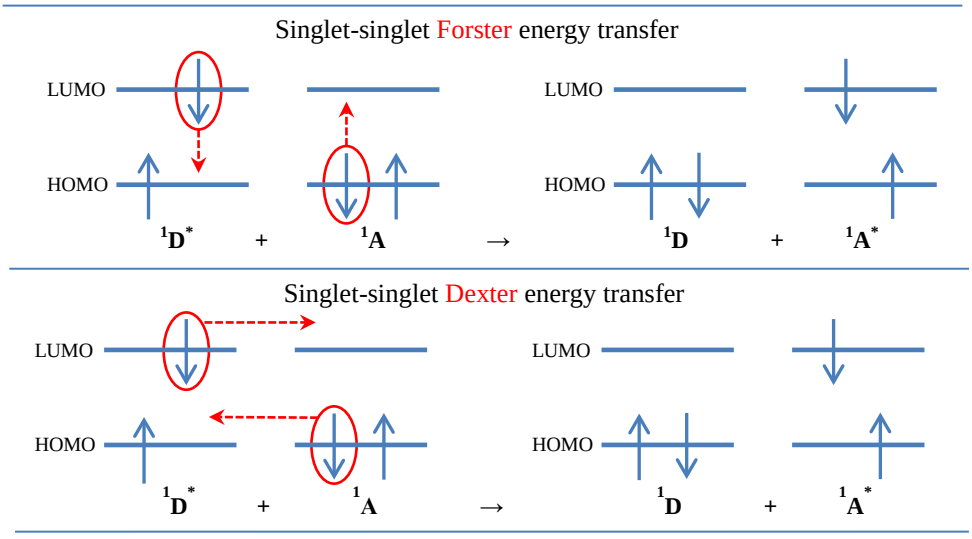

Figure 5.1: Mechanism of Forster energy transfer and Dexter energy transfer.

Fluorescence study on self-quenching of squaraines could be used to study the exciton diffusion, since squaraines may also quench by a mechanism of Förster energy transfer. We are also interested in the impact of doping PCBM on fluorescence properties because it is used as an electron acceptor in OPV devices. We have observed that PCBM could disrupt the formation of aggregates. Thus it is worth comparing the quenching effect of self-quenching and $DiBSQ(OH)_2$ to PCBM quenching. A Stern-Volmer like treatment is used as the tool.

In a standard Stern-Volmer plot[40] I_o/I is shown as a function the concentration of quencher (***equation 5.1***).

$$\frac{F_o}{F} = \frac{QY_o}{QY} = \frac{k_r^o/(k_r^o+k_{nr})}{k_r^o/(k_r^o+k_{nr}+k_Q[PCBM])} = \frac{k_r^o+k_{nr}+k_Q[PCBM]}{k_r^o+k_{nr}} = 1 + \frac{k_Q[PCBM]}{k_r^o+k_{nr}} \quad \textbf{Equation 5.1}$$

where F and F_o are fluorescence with and without presence of quencher, respectively. QY_o and QY are correlated quantum yield, k_r^o is the natural radiative rate constant, k_{nr} is the rate constant for all of the monomolecular nonradiative process, the k_Q is rate constant of quenching, and $[PCBM]$ is the concentration of quencher, which is PCBM in this case.

This standard Stern-Volmer plot is not used in this exact form is because: (1) this derivation is not valid for self-quenching since the intensity of fluorescence increases due to the increase of fluorophore, but at the same time it decreases due to the self-quenching interaction; (2) the effect of self-quenching on the Stern-Volmer constant as a function of the concentration of fluorophore ($DiBSQ(OH)_2$) is not considered, the stern-volmer equation is then modified by taking the self-quenching into account (***equation 5.2***):

$$\frac{I_o}{I} = \frac{QY_o}{QY} = \frac{k_r^o/(k_r^o+k_{nr}+k_{SQ}[DIBSQ(OH)_2])}{k_r^o/(k_r^o+k_{nr}+k_{SQ}[DIBSQ(OH)_2]+k_Q[PCBM])} =$$

$$\frac{k_r^o+k_{nr}+k_{SQ}[DIBSQ(OH)_2]+k_Q[PCBM]}{k_r^o+k_{nr}+k_{SQ}[DIBSQ(OH)_2]} = 1 + \frac{k_Q[PCBM]}{k_r^o+k_{nr}+k_{SQ}[DIBSQ(OH)_2]} \quad \textbf{(Equation 5.2)}$$

As the equation above shows when self-quenching is considered, the Stern-Volmer coefficient which is $k_{SV} = \frac{k_Q}{k_r^o+k_{nr}+k_{SQ}[DIBSQ(OH)_2]}$ will vary when the concentration of squaraine is varied and this is not good for comparison of the PCBM-squaraine

quenching effect when concentration of squaraine is different.

Since the data of absolute quantum yields are already collected, a Stern-Volmer like plot is then made by plotting 1/QY VS concentration of quencher. Derivation of this plot is shown below:

$$QY = \frac{k_r^o}{k_r^o + k_{nr} + k_{SQ}[DIBSQ(OH)_2] + k_Q[PCBM]} \quad \textbf{(Equation 5.3)}$$

Rearrange the equation:

$$\frac{1}{QY} = \frac{k_r^o + k_{nr} + k_{SQ}[DIBSQ(OH)_2] + k_Q[PCBM]}{k_r^o} = \frac{k_r^o + k_{nr}}{k_r^o} + \frac{k_{SQ}[DIBSQ(OH)_2]}{k_r^o} + \frac{k_Q[PCBM]}{k_r^o}$$

$$= \frac{1}{QY_o} + \frac{k_{SQ}[DIBSQ(OH)_2]}{k_r^o} + \frac{k_Q[PCBM]}{k_r^o} \quad \textbf{(Equation 5.4)}$$

We can rewrite the equation when (1) concentration of DiBSQ(OH)$_2$ is varied while PCBM absent, and (2) concentration of PCBM varied while [DiBSQ(OH)$_2$] fixed.

$$(1): \frac{1}{QY} = \frac{1}{QY_o} + \frac{k_{SQ}[DIBSQ(OH)_2]}{k_r^o} \quad \textbf{(Equation 5.5)}$$

$$(2): \frac{1}{QY} = constant + \frac{k_Q[PCBM]}{k_r^o} \quad \textbf{(Equation 5.6)}$$

The rate constants of (1) self-quenching, k_{SQ}, and (2) DiBSQ(OH)$_2$ to PCBM quenching, k_Q, thus can be presented by Stern-Volmer constant $K_{SV} = k_{SQ}/k_r^o$ and $K_{SV} = k_Q/k_r^o$, and given that k_r^o is constant, the quenching effect can now be directly compared using this Stern-Volmer like approach.

5.2 Experiments and results

To investigate the impact of self-quenching in the solid state, DiBSQ(OH)$_2$ films are spin-cast with PMMA. The weight ratio of DiBSQ(OH)$_2$ to PMMA is varied. To compare the quenching effect of self-quenching with the quenching of DiBSQ(OH)2 with PCBM, films containing DiBSQ(OH)$_2$, PCBM, and PMMA are spin-cast in ternary blends. In this case, the concentration of DiBSQ(OH)$_2$ is fixed while the relative amount of PCBM is varied. The Quantum Yield of thin films is measured using the set up as described in chapter 2 (***figure 2.1***). A special film holder for integration sphere is

used. In order to put the films into this holder, films about to be measured are cut into appropriate size using a glass cutter.

a) Self-quenching of $DiBSQ(OH)_2$

A plot of the reciprocal of the quantum yield of the film as a function of the concentration of the $DiBSQ(OH)_2$ is shown in ***figure 5.2***. The self-quenching is apparent once the concentration has increased beyond ~0.008 mol/L. As a result, the quantum yield of fluorescence decreases quickly and eventually drops down to zero when the concentration exceeds $DiBSQ(OH)_2$ 0.04M/L.

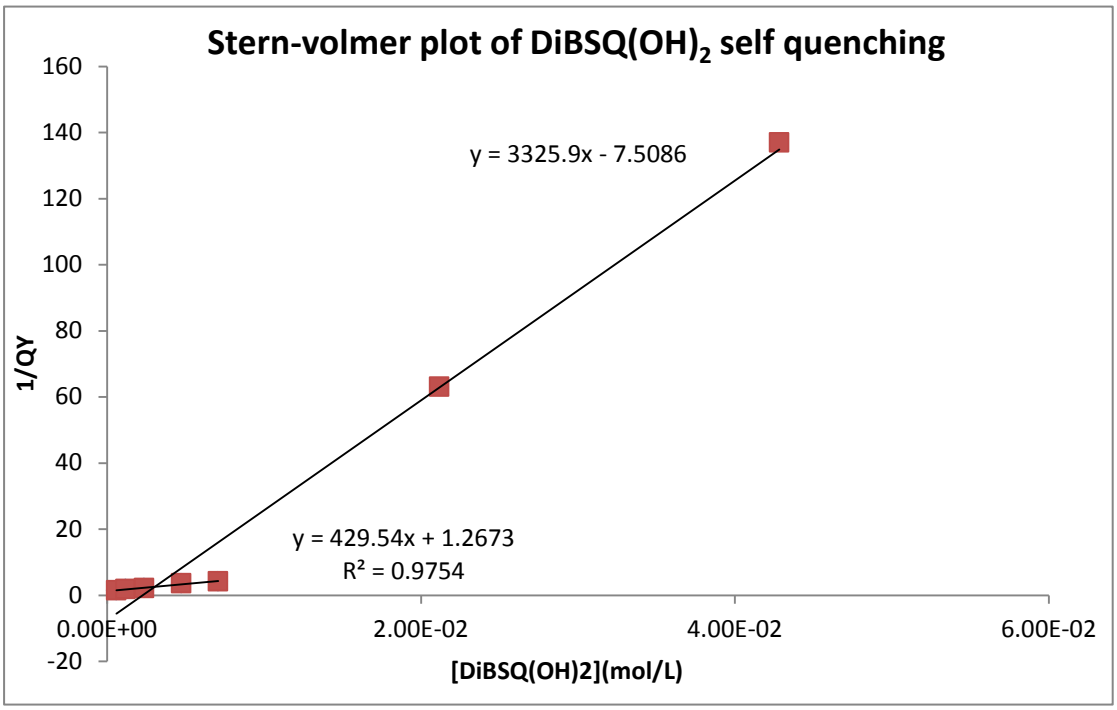

Figure 5.2: Stern-Volmer plot for self-quenching of $DiBSQ(OH)_2$.

b) quenching of $DiBSQ(OH)_2$ by PCBM in solid solution blends when the concentration of $DiBSQ(OH)_2$ is low:

When the concentration of squaraine is kept at a value low enough such that monomers might dominate, and such that self-quenching is minimal, a slope of 759 L/mol PCBM is observed **(*figure 5.3*)**. A straight line fits the data relatively well but we can also see that this data could be described by two lines with an intersection at about

$2 \times 10^{-4} mol/L.$

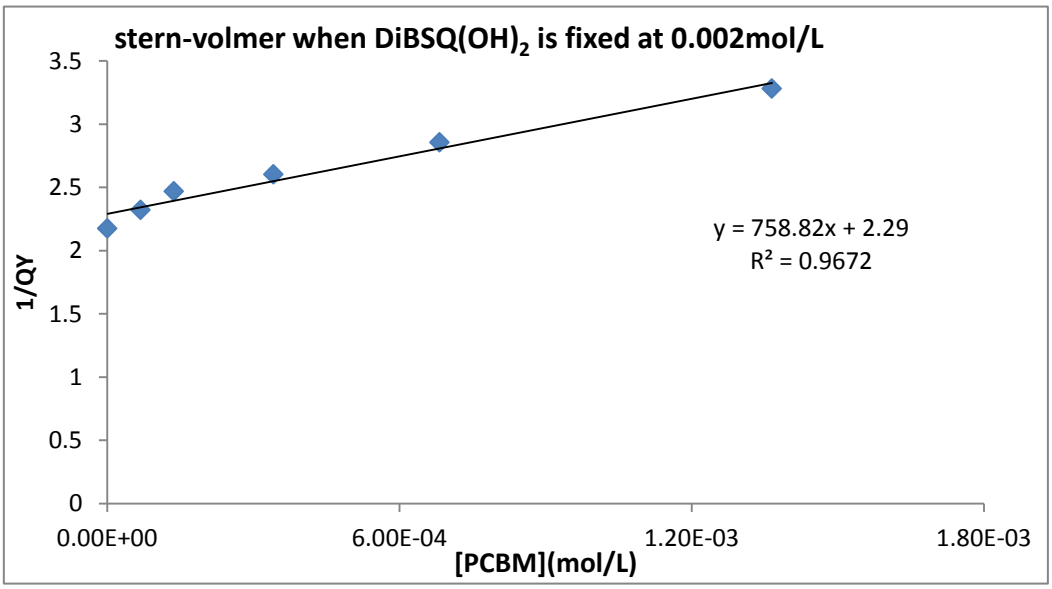

Figure 5.3: A graph showing the reciprocal of the quantum yield as a function of the PCBM concentration in a PMMA solid solution of 0.002 mol/L $DiBSQ(OH)_2$.

c) quenching of $DiBSQ(OH)_2$ to PCBM in solid solution when concentration of $DiBSQ(OH)_2$ is high:

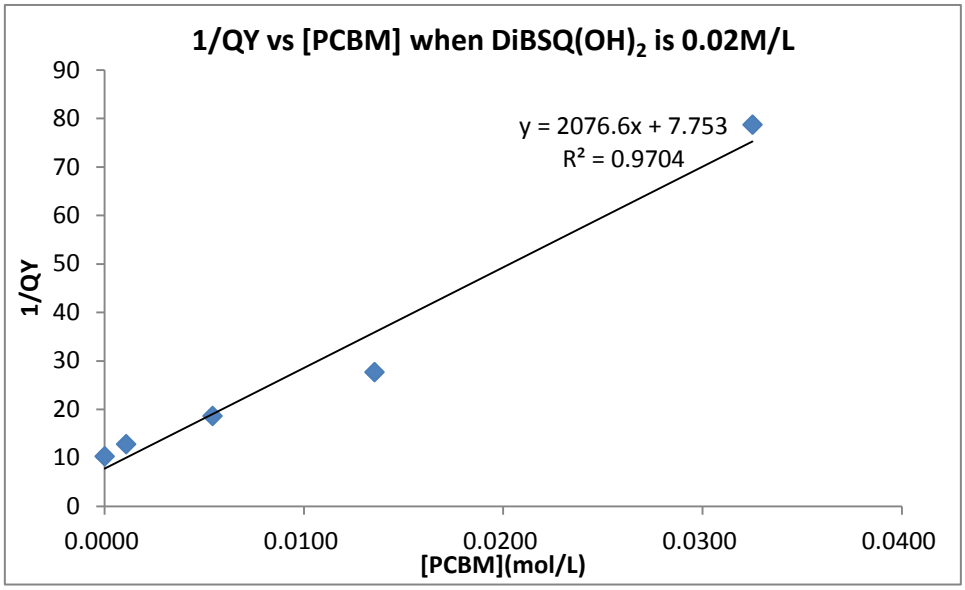

Figure 5.4: A graph showing the reciprocal of the quantum yield as a function of the PCBM concentration in a PMMA solid solution of 0.02 mol/L $DiBSQ(OH)_2$.

When the concentration of squaraine is kept at a value high enough such that aggregates might dominate, a slope of 2080±207 L/mol PCBM is observed. A straight

line fits the data relatively well.

5.3 Discussion

a) Self-quenching of DiBSQ(OH)$_2$

As with absorption, the three squaraines under investigation all show similar fluorescence spectra in dilute solid solution (***figure 5.5***). The λ_{max} of the fluorescence spectrum for DiBSQ(OH)$_2$ red shifts from 662nm in solution to 674nm in PMMA film. This may be due to the effect of re-absorption, since the concentration of the squaraine dye in PMMA film is much higher than in solution.

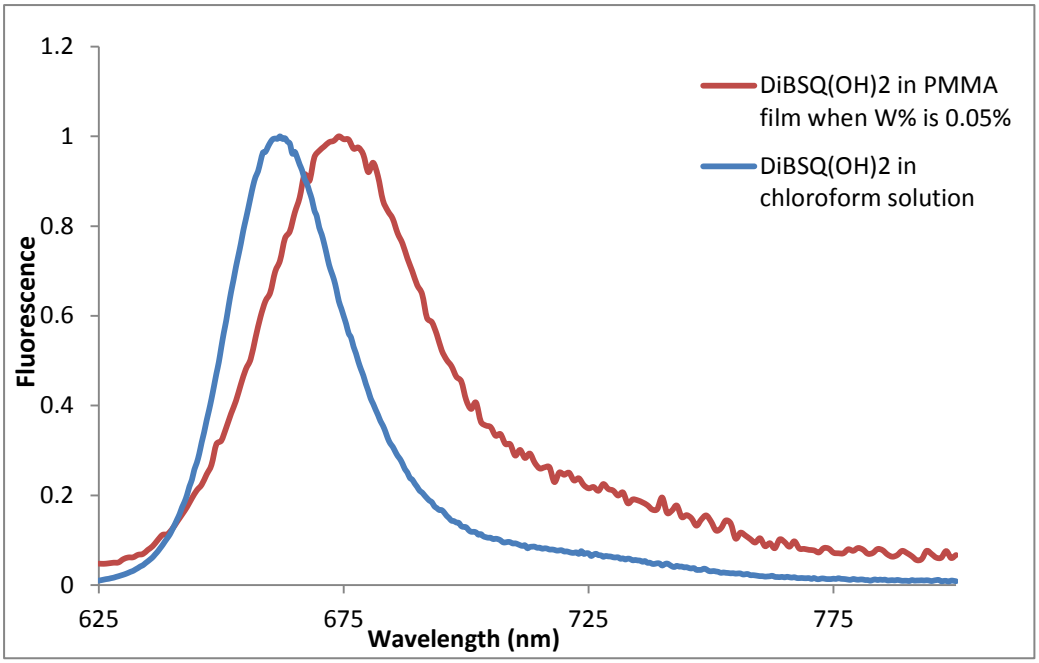

Figure 5.5: Fluorescence spectra of DiBSQ(OH)$_2$ in solution (blue line) and in PMMA film (red line).

Fluorescence is detected only when the ratio of squaraine weight to PMMA weight is smaller than 1%. For the films with the least concentration of squaraine, the quantum yield of squaraine fluorescence in solid solution is slightly higher than in liquid solution. This can be explained by the frozen molecular structure of squaraine, which minimizes vibrational relaxations. As the concentration of squaraine increases in PMMA solid solution, the quantum yield decreases sharply and eventually down to zero when the

weight ratio exceeds 1%. The sharp decrease is assigned to self-quenching.

As predicted by equation: $\frac{1}{QY} = constant + \frac{k_{SQ}[DIBSQ(OH)_2]}{k_r^o}$, a straight line with constant slope (concentration independent) is predicted in a Stern-Volmer plot, in which the slope is defined as the Stern-Volmer constant $K_{SV} = k_{SQ}/k_r^o$. However, in ***figure 5.2***, the Stern-Volmer constant (K_{SV}) of DiBSQ(OH)$_2$ self-quenching is found to be concentration dependent. The Stern-Volmer constant is determined as 429 L/mol when the concentration of DiBSQ(OH)$_2$ is smaller than 0.007mol/L in PMMA thin film; when concentration of DiBSQ(OH)$_2$ is higher than 0.02ml, K_{SV} increases to 3325 L/mol, which is almost 8 times the value at relatively low concentration. Because in PMMA film the molecules are fixed under solid state, dynamic quenching mechanism must be ruled out. We propose to attribute this interesting result to formation of long range aggregates, which act as a stronger quenchers than the monomer itself. Unlike the H-and J- aggregate forms discussed before, this long range aggregate is not significantly affecting the absorbance spectrum; it only leads to a de-excitation of the excited states. Based on the Stern-Volmer plot, an increase in the quenching rate constant occurs when the concentration of DiBSQ(OH)$_2$ exceeds 0.02mol/L, which gives an average intermolecular distance of 4.28nm, as determined from ***equation 4.1*** and ***equation 4.2***.

b) PCBM quenching with DiBSQ(OH)$_2$

Two Stern-Volmer like plots of the quenching effect of PCBM to DiBSQ(OH)$_2$ are presented in ***figure 5.3*** and ***figure 5.4***. When the concentration of PCBM is varied from $1 \times 10^{-4} mol/L$ to $2 \times 10^{-3} mol/L$ and DiBSQ(OH)$_2$ is fixed at $2 \times 10^{-3} mol/L$, the Stern-Volmer slope is 759. However, when concentration of PCBM is varied from $2 \times 10^{-3} mol/L$ to $5 \times 10^{-2} mol/L$ and DiBSQ(OH)$_2$ is fixed at $2 \times 10^{-2} mol/L$, the Stern-Volmer slope is a considerably larger 2076 units. We were considering PCBM as an aggregate disruptor, thus expecting the K_{sv} value to perhaps decrease as the concentration of PCBM increases. A likely trend can be found in ***figure 5.3***, where two

lines could fit as well. As a matter of fact, K_{sv} value is higher when both the concentration of PCBM and $DiBSQ(OH)_2$ is higher. Since förster energy transfer between PCBM and $DiBSQ(OH)_2$ is not likely to happen because the energy gap of PCBM is higher than $DiBSQ(OH)_2$. This might suggest that either a PCBM-$DiBSQ(OH)_2$ complex is formed or as the concentration of PCBM increases, the aggregation of $DiBSQ(OH)_2$ is favored probably due to the phase separation which is enhanced by adding PCBM. For future studies, annealing experiments can be used. If a complex is being formed, then after annealing the quantum yield of the film should not be changed. If PCBM is enhancing aggregation of $DiBSQ(OH)_2$ due to phase separation, then annealing should enhance the phase separation, which is going to form more aggregate.

c) Proof of PCBM interact with squaraine

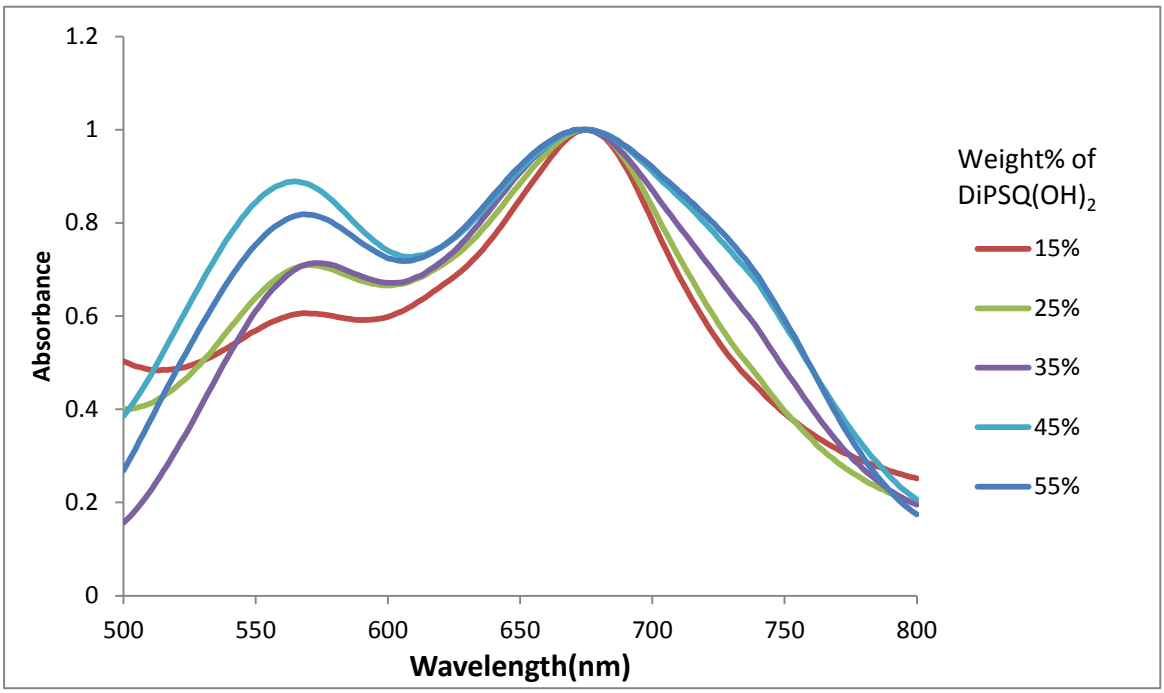

Figure 5.6: Absorbance spectra of $DiPSQ(OH)_2$ – PCBM films.

Thin films made in a blend of $DiPSQ(OH)_2$ with PCBM were spin cast. The absorption spectra of these blended films are shown in ***figure 5.6***. There are two main peaks observed, one at ~680nm and the other at ~570nm. The peak at 680nm is

assigned to the monomer and that at 570nm is assigned to the H-aggregate. These assignments are made based upon the similar assignments made in ***figure 4.4***. More importantly, when ***figure 5.6*** is compared with ***figure 4.4***, the J-aggregate peak which has a λ_{max} at 745nm in the absorbance spectra of DiPSQ(OH)$_2$-PMMA films (***figure 4.4***) is no longer observed in the absorbance spectra of DiPSQ(OH)$_2$-PCBM films (***figure 5.6***). The PCBM appears to completely disrupt the formation of the J-aggregate of DiPSQ(OH)$_2$.

5.4 Conclusion

To optimize the efficiency of OPV devices, understanding the process of exciton diffusion is essential. Fluorescence study is a practical tool. However, it requires fluorescence emission, which is not detected on our working devices. PMMA films are spin casted for fluorescence study. Based on the fact that the Stern-Volmer slop increase as the concentration of squaraine increases, we conclude some kind of long-range aggregate forms in solid state. Doting PCBM into PMMA films turns out an obstruction on fluorescence of squaraines. It could be explained by either formation of PCBM-squaraine complex or enhancing phase separation which results in more squaraine aggregate formed. For future study, annealing experiment and TCSPC can be used.

Chapter 6

Aggregation of squaraines in mixed aqueous-organic solution

6.1 Introduction

To further investigate the properties of the squaraine dyes, the aggregation behavior of squaraines in aqueous-organic cosolvent mixtures is studied. Compared with a photophysical study on thin films in general, solution studies are advantageous because (1) a solution is easier to be prepared than a thin film and uses relatively small amounts of materials and (2) a solution is in a homogeneous phase the properties of which can be easily controlled by changing the relative volume percentages of the two solvents. Furthermore a lot of information can easily and reproducibly be obtained through absorption spectrum measurements, largely because of the well-defined path length.

Aggregation occurs in solution when the squaraines have a large enough enthalpic driving force to condense as opposed to the enthalpic driving force of interacting favorably with the solvent combined with the entropic gains of full solubility. There of course is an equilibrium point for any solution and the associated aggregation. The equilibrium between monomer (**M**) and aggregate (**Agg**) of order *n* can be analyzed by the Benesi-Hildebrand treatment[41] according to the following equation.

$$\ln \boldsymbol{I}_a = n \ln(\boldsymbol{I}_{ao} - \boldsymbol{I}_a) + \text{constant} \qquad \textbf{(Equation 6.1)}$$

where I_a is the absorbance of aggregate in solution mixture at a certain concentration and I_{ao} is the absorbance of aggregate only (no monomer present) when all the monomers are converted into aggregates for this certain concentration. The analyses are based on the assumption that the relationship between the monomer and the aggregate

can be described by equilibrium constant and be represented by the following stoichiometry:

$$n\mathbf{M} \rightleftharpoons \mathbf{Agg} \qquad \textbf{(Equation 6.2)}$$

where **M** is monomer, **Agg** is aggregate, this reaction has an equilibrium constant:

$$K=[\mathbf{Agg}]/[\mathbf{M}]^n \qquad \textbf{(Equation 6.3)}$$

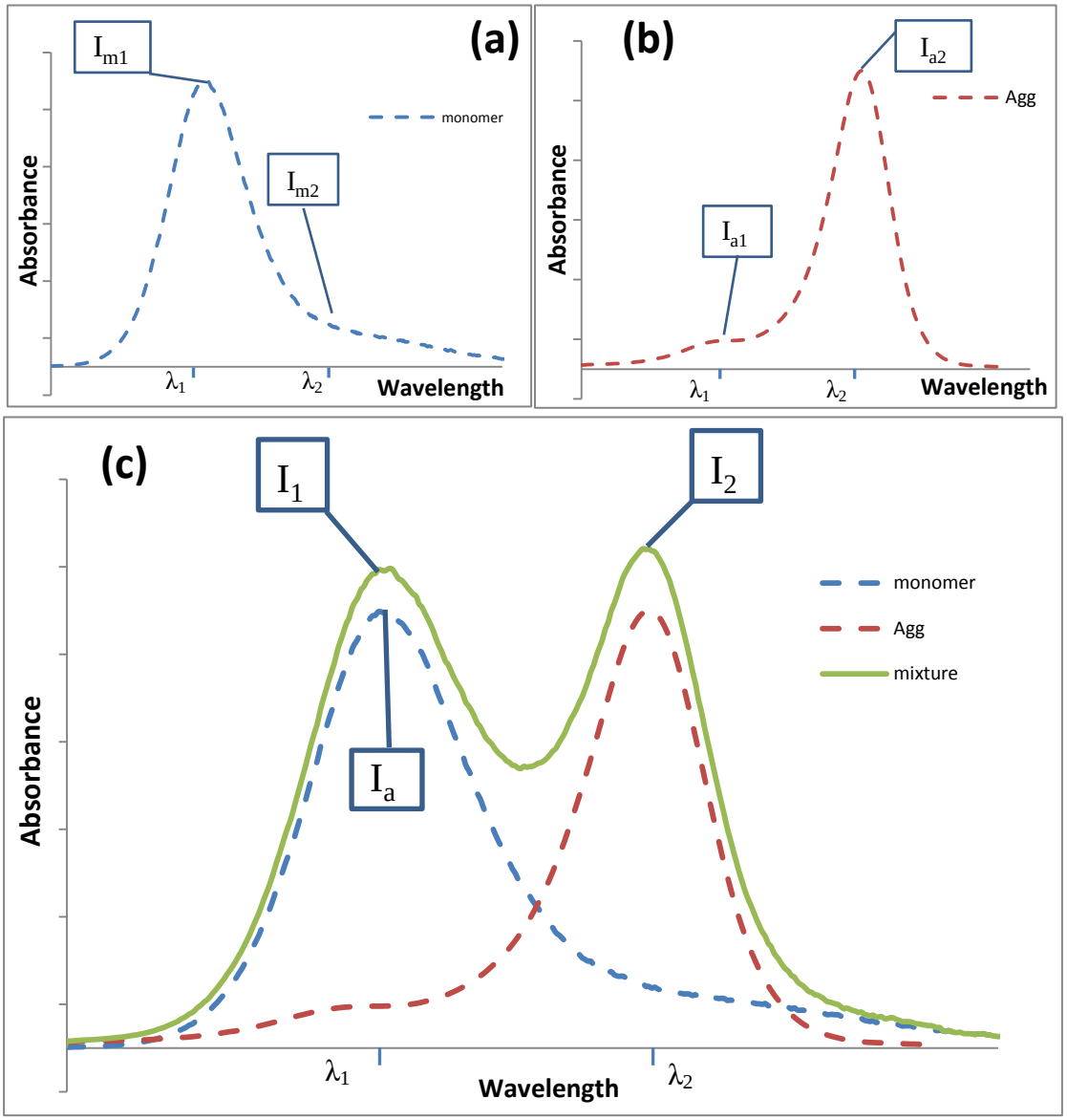

Figure 6.1: Absorbance spectra when only monomer is present (**a**), only pure aggregate present (**b**), and when monomer and aggregate are mixed in solution (**c**).

The monomer spectrum and the pure aggregate spectrum were characterized by experiment. The monomer spectrum has an absorbance maximum peak at λ_1, the pure aggregate spectrum has an absorbance peak at λ_2. It is assumed that the absorbance in the monomer spectrum for each wavelength λ_1 and λ_2 is I_{m1} and I_{m2}, respectively, and

that the absorbance in the aggregate spectrum for each wavelength λ_1 and λ_2, is I_{a1} and I_{a2}, respectively. R_a and R_m are defined as the ratios of absorbance at wavelengths λ_1 and λ_2 for each of the monomer (R_m) and pure aggregate (R_a) spectra ***(figure 6.1)***:

$$R_m=I_{m1}/I_{m2} \quad \textbf{(Equation 6.4)}$$

$$R_a=I_{a1}/I_{a2} \quad \textbf{(Equation 6.5)}$$

I_a can be found by equation:

$$I_a=R_a(I_1-R_mI_2)/(R_a-R_m) \quad \textbf{(Equation 6.6)}$$

The extinction coefficient of aggregate (**Agg)** must be found by experiment:

$$I_{ao}=\varepsilon_aC_0/n \quad \textbf{(Equation 6.7)}$$

I_{ao} is the absorbance at λ_{max} of pure aggregate spectrum, ε_a is the extinction coefficient, C_0/n is the concentration of aggregate when all the monomers have been transformed into aggregates.

Thus we have:

$$[\mathbf{Agg}]=I_a/n\varepsilon_a \quad \textbf{(Equation 6.8)}$$

$$[\mathbf{M}]=C_0-n[\mathbf{Agg}] =(I_{ao}-I_a)/\ \varepsilon_a \quad \textbf{(Equation 6.9)}$$

By plugging these two equations above into the equation $K=[\mathbf{Agg}]/[\mathbf{M}]^n$, or $[\mathbf{Agg}]=K[\mathbf{M}]^n$:

$$I_a/n\varepsilon_a=K[(I_{ao}-I_a)/\varepsilon_a]^n \quad \textbf{(Equation 6.10)}$$

This can be written in:

$$I_a=[(I_{ao}-I_a)]^n(nK/\varepsilon_a{}^{n-1}) \quad \textbf{(Equation 6.11)}$$

Taking natural logs on both sides:

$$\ln I_a=n\ln(I_{ao}-I_a)+\ln(nK/\varepsilon_a{}^{n-1}) \quad \textbf{(Equation 6.12)}$$

Noticing that $\ln(nK/\varepsilon a^{n-1})$ is constant, the equation above can be written as:

$$\ln I_a=n\ln(I_{ao}-I_a)+\text{constant} \quad \textbf{(Equation 6.13)}$$

Hence, the aggregate number, n, can be determined by plotting $\ln I_a$ as a function of $\ln(I_{ao}-I_a)$.

6.2 Experiments and Results

a) Aggregate properties of DiPSQ(OH)$_2$ in solutions

The aggregate properties of DiPSQ(OH)$_2$ were investigated as a function of solvent composition using a series of organic solvent-water mixtures. Solutions are freshly prepared before being measured by UV-VIS spectrometer. When acetonitrile-water and DMA-water cosolvent systems were used, two characteristic aggregate peaks with λ_{max} at 550nm and 760nm were observed when the volume ratio of water increased from 26% to 35% (***figure 6.2a***). The obtained aggregate peak of DiPSQ(OH)$_2$ (***figure 6.2a***) in mixed solvents matches well with the aggregate spectra obtained in PMMA films (***figure 4.4***). A comparison of absorbance spectra of DiPSQ(OH)$_2$ in mixed solvents and in PMMA films is made in ***figure 6.2c***. Although future work needs to be done to prove the aggregate in solution and that in PMMA films are the same species, it's reasonable to assume that they are the same at this point.

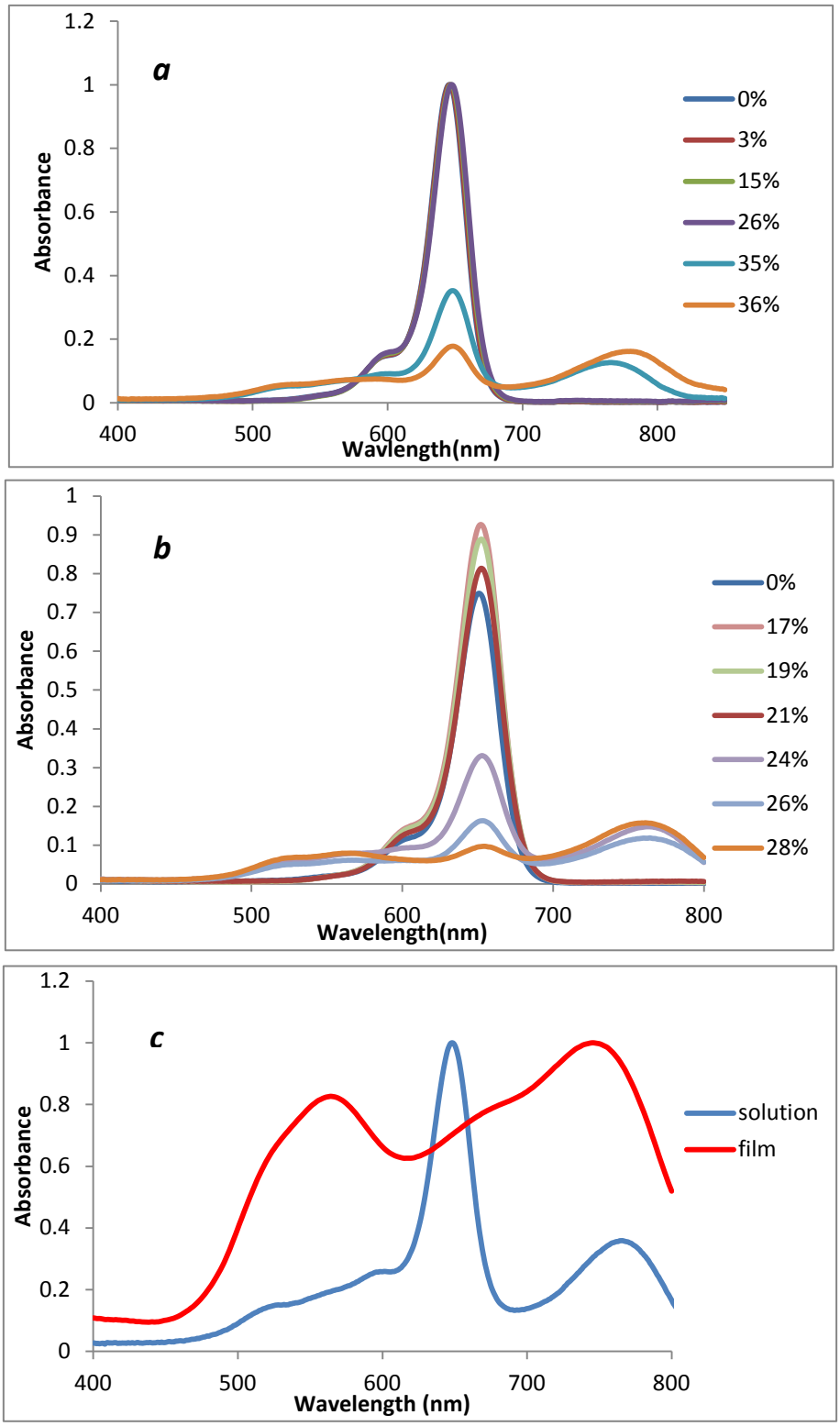

Figure 6.2: Graph showing the absorbance of various solutions of DiPSQ(OH)$_2$ in acetone-water mixed solvents with varying percentages of water (***a***), the absorbance of various solutions of DiPSQ(OH)$_2$ in DMA-water mixed solvents with varying percentages of water (***b***), absorbance of DiPSQ(OH)2 in solution and in films compared in one plot.

b) Determine the aggregate number *n* of DiPSQ(OH)$_2$

To determine the aggregate number *n* by Benesi-Hildebrand treatment, the

concentration of DiPSQ(OH)$_2$ was varied while the constituents of the cosolvent mixture were kept the same. Since the concentration of DiPSQ(OH)$_2$ needs to be varied, the solubility of DiPSQ(OH)$_2$ in the cosolvent becomes crucial. As water is added into the solvent, the solubility of DiPSQ(OH)$_2$ keeps decreasing. Eventually DiPSQ(OH)$_2$ will crash out as a precipitate at some point. Nevertheless, aggregation of DiPSQ(OH)$_2$ in solvent mixtures happens when close to the critical point of crashing out. At such a point, even adding just a small amount of DiPSQ(OH)$_2$ may break the equilibrium and cause precipitation. For example, in ***figure 6.3***, when a DMA-acetone-water solution is used, DiPSQ(OH)$_2$ crashes out of solution and a precipitate is observed as only 0.02mg more of DiPSQ(OH)$_2$ is added. As a result, the monomer peaks became much lower. This feature makes an appropriate cosolvent important since now we are walking on the edge of adding more DiPSQ(OH)$_2$ into the solution but also need to keep DiPSQ(OH)$_2$ from precipitating. After many kinds of combination of organic solvent and water have been tried, DMA-acetonitrile-water were chosen because this system could tolerate enough DiPSQ(OH)$_2$ for Benesi-Hildebrand treatment while keeping DiPSQ(OH)$_2$ from crashing out.

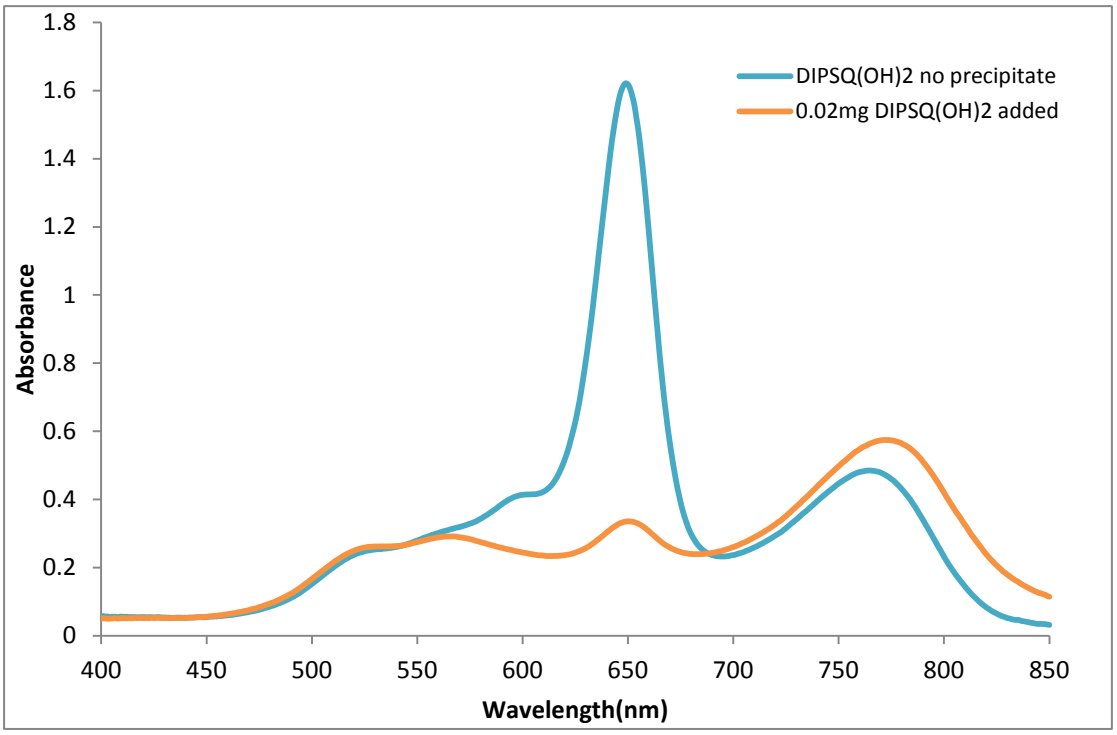

Figure 6.3: DiPSQ(OH)$_2$ crashed out (orange line) when only 0.02mg more of solute was added.

c) Aggregate properties of DiBSQ(OH)$_2$ in solutions

The aggregate properties of DiBSQ(OH)$_2$ were also investigated as a function of solvent composition using organic solvent-water mixtures. Absorbance spectra of DiBSQ(OH)$_2$ in DMA-water and acetonitrile-water solvent mixtures were recorded; the volume ratio of water was varied from 0% to 33%, respectively. No significant sign of an aggregate peak was observed for this squaraine in organic solvent-water mixtures (***figure 6.4***).

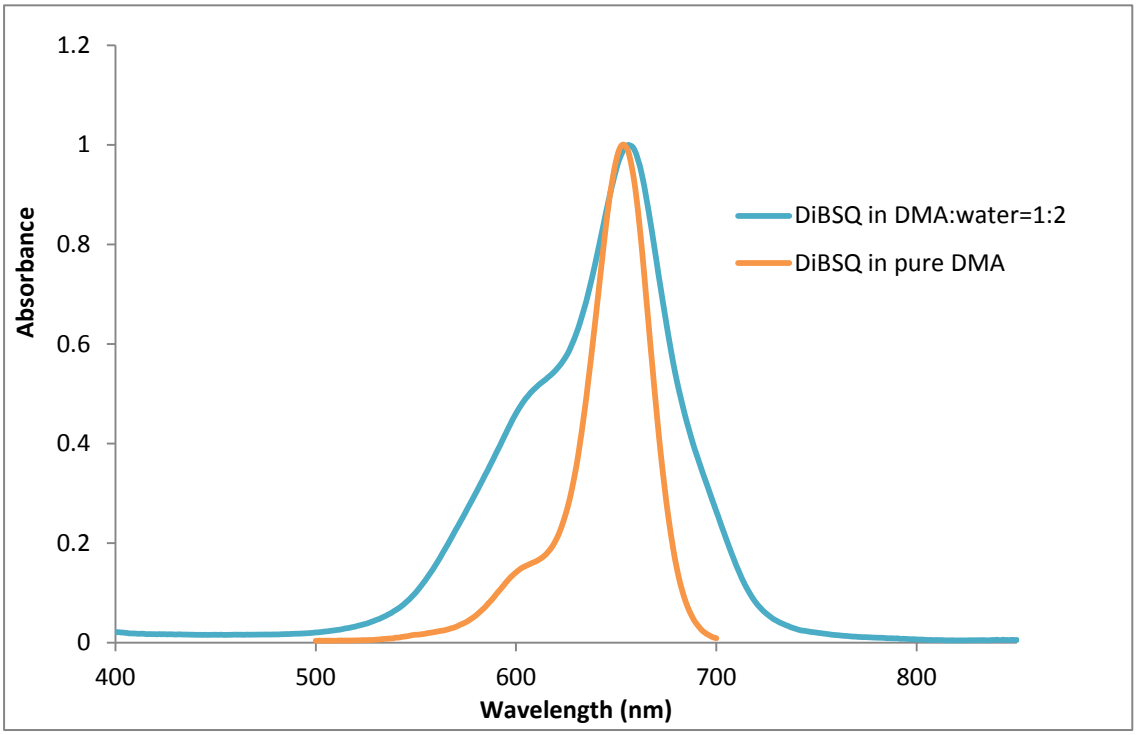

Figure 6.4: Absorbance spectrum of DiBSQ(OH)$_2$ in DMA-water mixture compared with the spectrum in pure DMA.

6.3 Discussion

a) Aggregation of DiPSQ(OH)$_2$ in solution

When DiPSQ(OH)$_2$ was dissolved in an acetone-water mixed solvent solution with varying ratios of water, the aggregate was observed when the volume of water increased from 26% to 35% of the total volume (***figure 6.2a***). A characteristic J-aggregate was identified with λ_{max} at 762nm when the water to acetone ratio was

equal to 35%. The aggregate peak red-shifted to 777nm when the ratio of water to acetone increased from 35% to 36% with just a 1% increment.

When $DiPSQ(OH)_2$ was dissolved to form a DMA-water mixed solvent solution with varying ratios of water, the aggregate was observed when the volume percentage of water increased from 21% to 24% (***figure 6.2b***). A characteristic J-aggregate was assigned to the absorbance feature with λ_{max} at 760nm when the water percentage was higher than 24%. Compared with the data from the corresponding acetone-water solvent mixtures experiment in part 1, the DMA-water solutions require less water for the aggregate to form and be observed.

Although it is well known that there are two different forms of aggregate which result in a blue-shift (H-aggregate) and a red-shift (J-aggregate) of the absorbance peak respectively, it may be possible that one aggregate gives a both red-shifted peak and a blue-shifted peak at the same time. If this hypothesis is true, then the height of H-aggregate peak at 550nm and J-aggregate peak at 760nm should keep the same ratio all the time. On the other hand, if the H-aggregate peak at 550nm and J-aggregate peak at 760nm come from two different aggregate species, then we can change the equilibrium between H-aggregate and J-aggregate by changing the ratio of constituent of cosolvent. As a result, the relative height of H-aggregate peak and J-aggregate peak should change as well.

The absorbance data for two solutions of $DiPSQ(OH)_2$ using mixtures of DMSO and water are shown in ***figure 6.5***. The impact of different volume ratios of water is shown. As the volume ratio of water is changed from 50% to 60% while the concentration of $DiPSQ(OH)_2$ remains the same, the relative height H-aggregate peak at 550nm and J-aggregate peak at 760nm changed as well. These data (***figure 6.5***) support the assumption that there are two different kinds of aggregate formed.

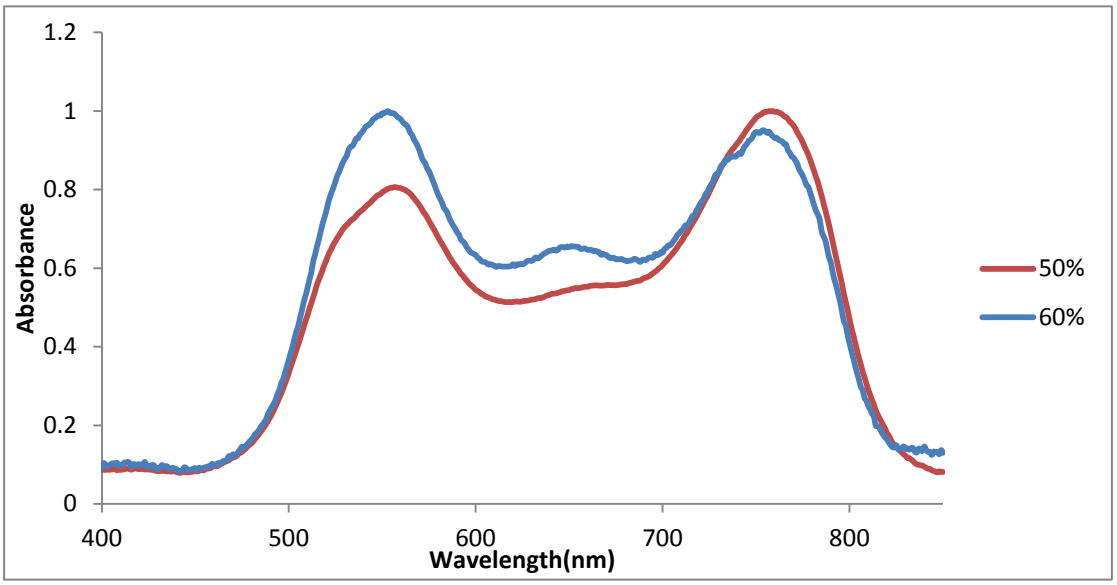

Figure 6.5: Two different aggregate spectra of $DiPSQ(OH)_2$ in DMSO-water cosolvent with same concentration of $DiPSQ(OH)_2$ but different volume ratio of water.

b) Aggregation of $DiBSQ(OH)_2$ in solution

Compared with the absorbance spectrum of $DiBSQ(OH)_2$ in pure DMA (***figure 6.4***), the absorbance peak of $DiBSQ(OH)_2$ in DMA-water mixtures is only slightly shifted (1nm red-shift). Although the two spectra are not exactly the same, such a change on the absorbance band is not distinctive and might be attributed to the influence of additional water. If we put all three spectra in one plot (***figure 6.6***), the absorbance peak of $DiBSQ(OH)_2$ in DMA-water mixtures is more like the monomer as in pure DMA, while differing more substantially from the aggregate features seen in the solid state.

Nevertheless, this experiment doesn't eliminate the possibility of $DiBSQ(OH)_2$ aggregates in solutions. This chapter's focus on $DiPSQ(OH)_2$ and the experiments tried on $DiBSQ(OH)_2$ are not sufficient to make a fully qualified conclusion in this respect. Still, these data are valuable for further digging on the aggregate properties of $DiBSQ(OH)_2$, which are revealed as interesting in chapter 4.

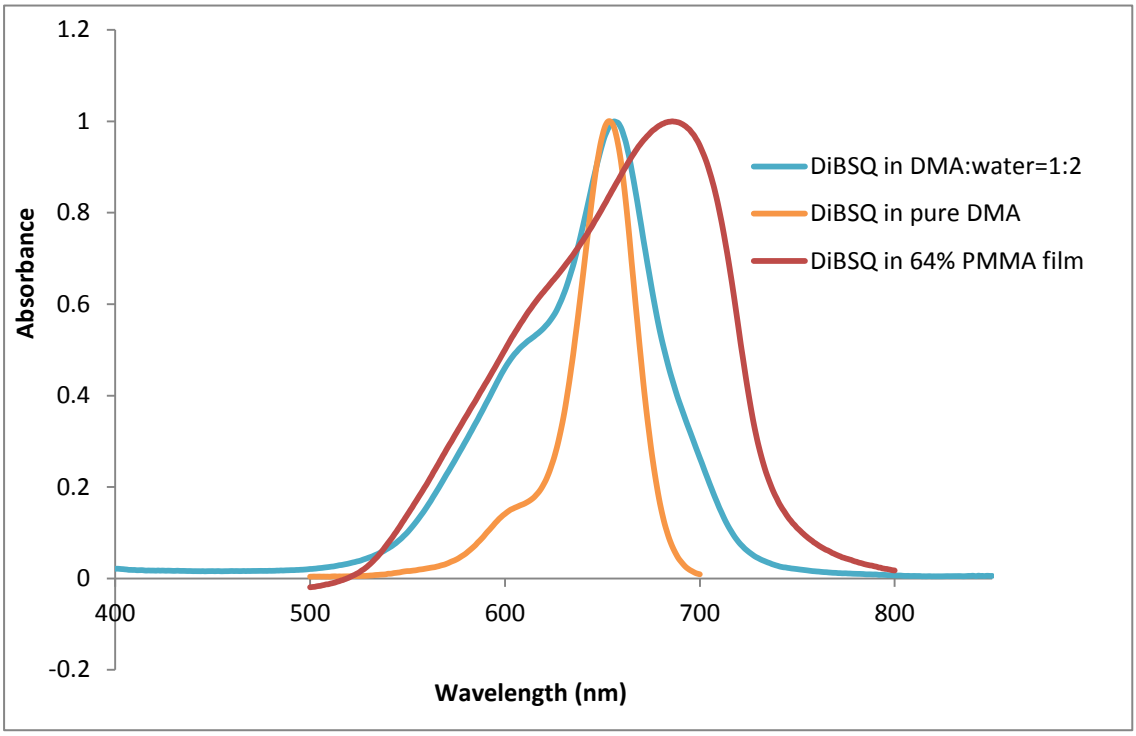

Figure 6.6: Absorbance spectrum of DiBSQ(OH)$_2$ in DMA-water cosolvent compared with the aggregate spectrum of DiBSQ(OH)$_2$ in PMMA film.

6.4 Benesi-Hildebrand treatment

To determine the aggregate number n of the J-aggregate of DiPSQ(OH)$_2$ by the Benesi-Hildebrand treatment, the concentration of DiPSQ(OH)$_2$ is varied while the ratio of DMA-acetonitrile-water mixture is fixed. The obtained spectra are presented in ***figure 6.7***. Since the overlap between monomer and aggregate peak is relatively small, it is reasonable to approximate the absorbance at the monomer peak (650nm) to be all from the monomer and the absorbance at the aggregate peak (760nm) to be all from the aggregate.

By Beer's Law, we have:

$$A_M = \varepsilon_M[\boldsymbol{M}]l \qquad \textbf{(Equation 6.14)}$$

$$A_{agg} = \varepsilon_{agg}[\boldsymbol{Agg}]l \qquad \textbf{(Equation 6.15)}$$

where A_M is the absorbance at the monomer peak (650nm), A_{agg} is the absorbance at the aggregate peak (760nm). When we plug these two equations into the Benesi-Hildebrand equation:

$$logK = \log[\boldsymbol{Agg}] - nlog[\boldsymbol{M}] \qquad \textbf{(Equation 6.16)}$$

an approximation equation is then obtained:

$$logK = log\frac{A_{agg}}{\varepsilon_{agg}l} - nlog\frac{A_M}{\varepsilon_M l} \quad \textbf{(Equation 6.17)}$$

Then we can rearrange the equation as:

$$logA_{agg} = nlogA_M - nlog\varepsilon_M l + log\varepsilon_{agg}l + logK \quad \textbf{(Equation 6.18)}$$

Given that the part of "$-nlog\varepsilon_M l + log\varepsilon_{agg}l + logK$" is constant, the aggregate number *n* can be solved by plotting $logA_{agg}$ as a function of $logA_M$ (***figure 6.8***). The aggregate number is determined as 2, suggesting a dimer for the J-aggregate of DiPSQ(OH)$_2$.

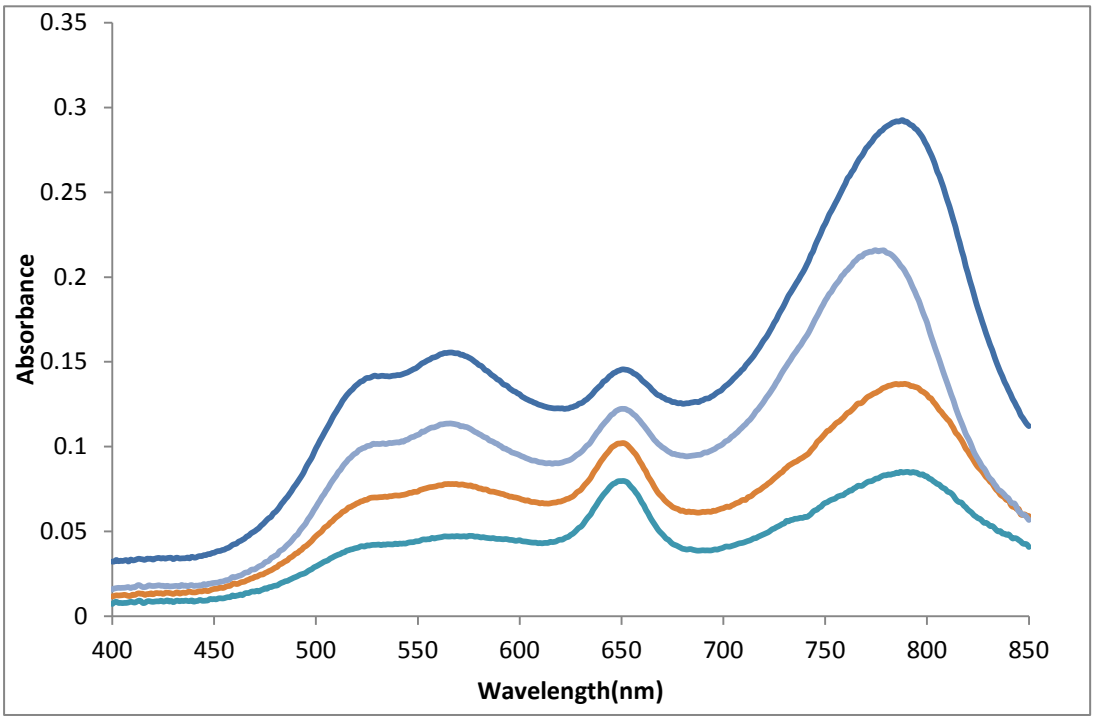

Figure 6.7: Absorption spectra for DiPSQ(OH)$_2$ in DMA-acetonitrile-H_2O mixture with varied concentration of DiPSQ(OH)$_2$.

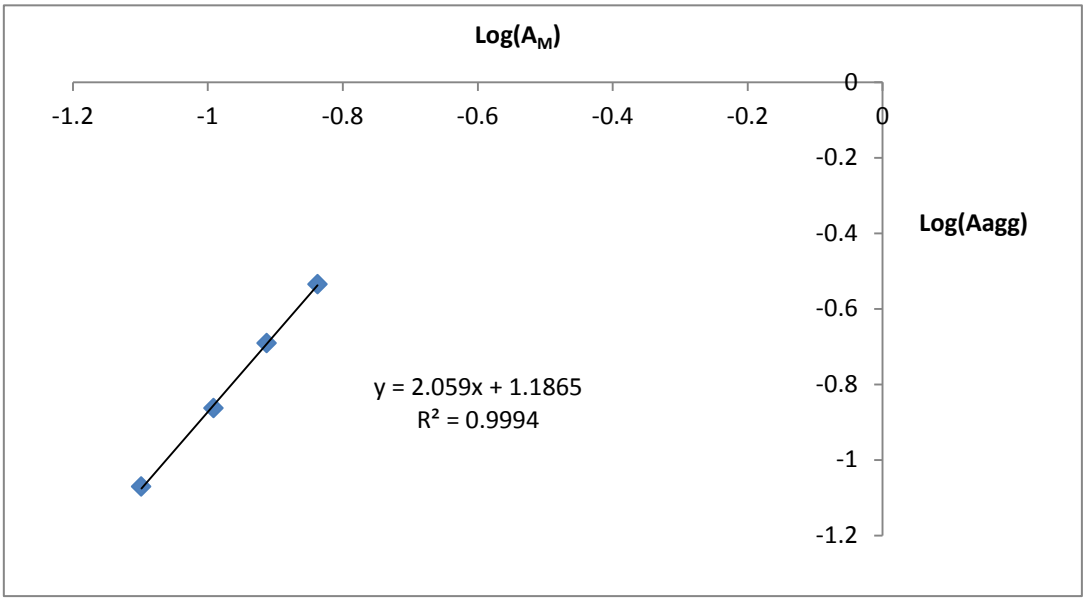

Figure 6.8: Benesi-Hilderbrand plot for J-aggregate of $DiPSQ(OH)_2$. *log*(A_M) as a function of *log*(A_{agg}) is plotted.

6.5 Conclusion

The aggregation of squaraines in solution is studied. The J-aggregate of $DiPSQ(OH)_2$ is characterized as a dimer (aggregate number 2). No aggregate is detected for $DiBSQ(OH)_2$, which is consistent with the interpretation that DiBSQ(OH)2 does not aggregate in chapter 3.

Chapter 7

PH dependence of squaraines

7.1 Introduction

Because of the unique structure, squaraines have been studied for a number of device applications. Recently Griffiths et. al.[42] have reported that the absorbance spectrum of squaraine is pH-sensitive, which makes squaraine a potential pH probe or indicator. Besides, the absorbance of squaraine is pH dependent because it reacts with base. This factor needs to be considered in OPV device making. This chapter provides information on how the absorbance spectrum of DiPSQ$(OH)_2$ changes as it reacts with NaOH.

7.2 Experiments

To investigate the effect of pH variation on squaraines, NaOH solution is added to solutions in ethanol. Ethanol is used as the solvent for NaOH because water is not soluble for most organic solvents. A NaOH stock solution (0.3mol/L) is firstly prepared. To obtain absorbance spectra of DiPSQ$(OH)_2$ in different PH, 3ml DiPSQ$(OH)_2$ solution is directly added into a cuvette, 0.01ml NaOH stock solution is directly added into the cuvette each time, the cuvette is shaken after the NaOH stock is added. Because the volume of the added NaOH stock is only 0.3% of entire solution, the volume of mixture can be approximated to be fixed as 3ml, thus the molarity of DiPSQ$(OH)_2$ is considered as constant while NaOH is varied.

7.3 Results and Discussion

1. The addition of NaOH (in ethanol) to DiPSQ(OH)$_2$ solution when ethanol is the solvent.

The volume of NaOH (in ethanol) added is a small fraction compared with total volume and therefore the molarity of DiPSQ(OH)$_2$ can be treated as a constant $2 \times 10^{-6} mol/L$. The molarity of the added NaOH solution is varied and is shown in the legend in ***figure 7.1***, where the absorbance spectra of the tested solutions are presented:

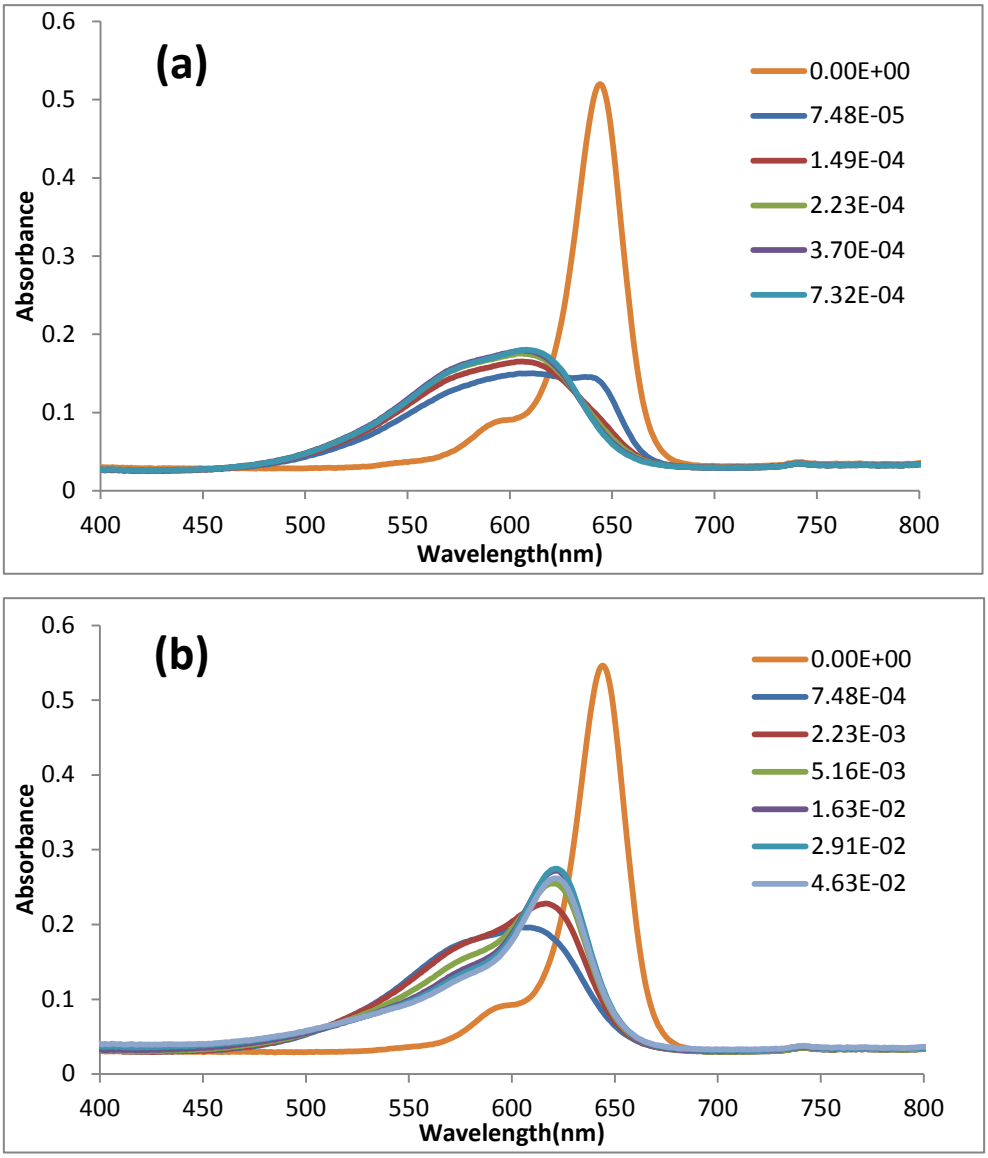

Figure 7.1: Absorbance spectra of DiPSQ(OH)$_2$ in ethanol and the effect of progressive addition of NaOH. Legend represents the concentration of NaOH. Molarity of NaOH is varied from zero to 7×10^{-4}mol/L (a), then keep increased up to 4×10^{-2}mol/L (b).

When the solution is neutral, the absorption band is sharp and intense. Once NaOH added ([NaOH] = 7×10^{-5}), the absorption peak of the neutral species (λ_{max} = 650nm) drops to one fifth of the original immediately, while a new absorption band (λ_{max} = 569nm) rises and eventually dominates until the molarity of NaOH is 7×10^{-4}. As the molarity of NaOH keeps increasing, the amount of species with λ_{max} = 569nm starts to decrease while another species (λ_{max} = 617nm) appears and shows increased absorbance until it is the only species in solution. These data are shown in ***figure 7.1***, with figure ***figure 7.1b*** following on from ***figure 7.1a***. We attribute the variation of spectra to the formation of de-protonated species. When NaOH added, $DiPSQ(OH)_2$ loses hydrogen cation, which breaks the symmetrical electrical structure and the intense sharp absorption band.

2. Adding NaOH (in ethanol) to $DiPSQ(OH)_2$ solution when DMA is the solvent.

Since there are four −OH group in one $DiPSQ(OH)_2$, then we would expect more de-proton species (lose two H^+ or even more) detected as PH increases. In order to see if furthermore de-protonated species can be detected, the solvent DMA is tried. The experimental method was the same as that described for part 1. Only the solvent was changed from ethanol to DMA. [$DiPSQ(OH)_2$] was fixed at a concentration of $6\times10^{-6}mol/L$. The results are shown in ***figure 7.2***.

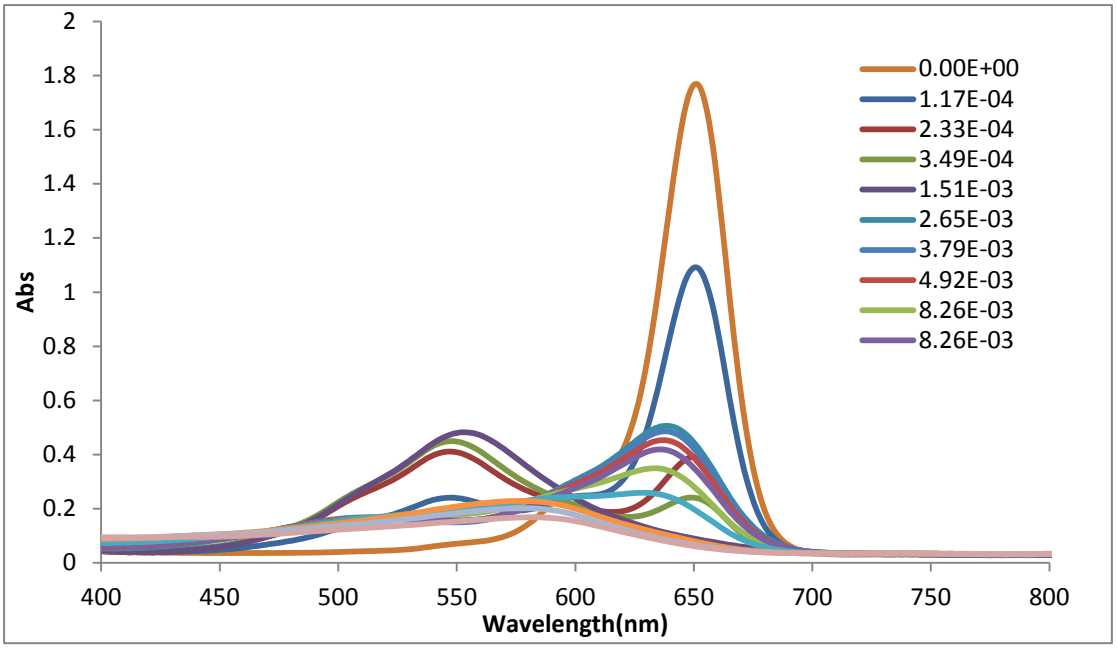

Figure 7.2: Absorbance spectra of DiPSQ(OH)$_2$ in DMA and the effect of progressive addition of NaOH.

Three species appear as the molarity of NaOH (pH) increases. The peak absorbance values for each of these species, which respectively grow in as pH increases, are 545nm, 634nm, and 571nm. The feature with a peak of 571nm is very broad.

A simplified plot of the species seen with neutral conditions along with the absorbance of the three "deprotonated" species is shown in ***figure 7.3***. Three species with different absorption bands came and went subsequently as the molarity of NaOH increased. The absorbance band at 545nm rose at first, followed by the one at 634nm, finally the species with an absorption band at 571nm dominates. A plot of the dominant value for the λ_{max} of absorption is provided as a function of pH in ***figure 7.4***. As ***figure 7.4*** shows, DiPSQ(OH)$_2$ could exist in three different ionic forms when pH varies. These ionic forms are a consequence of losing hydrogen cations. Since there are four hydroxyl groups (−OH) on a DiPSQ(OH)$_2$ squaraine, there might be one ultimate de-protonated subspecies of DiPSQ(OH)$_2$ when all four hydroxyl groups have lost their hydrogen ions.

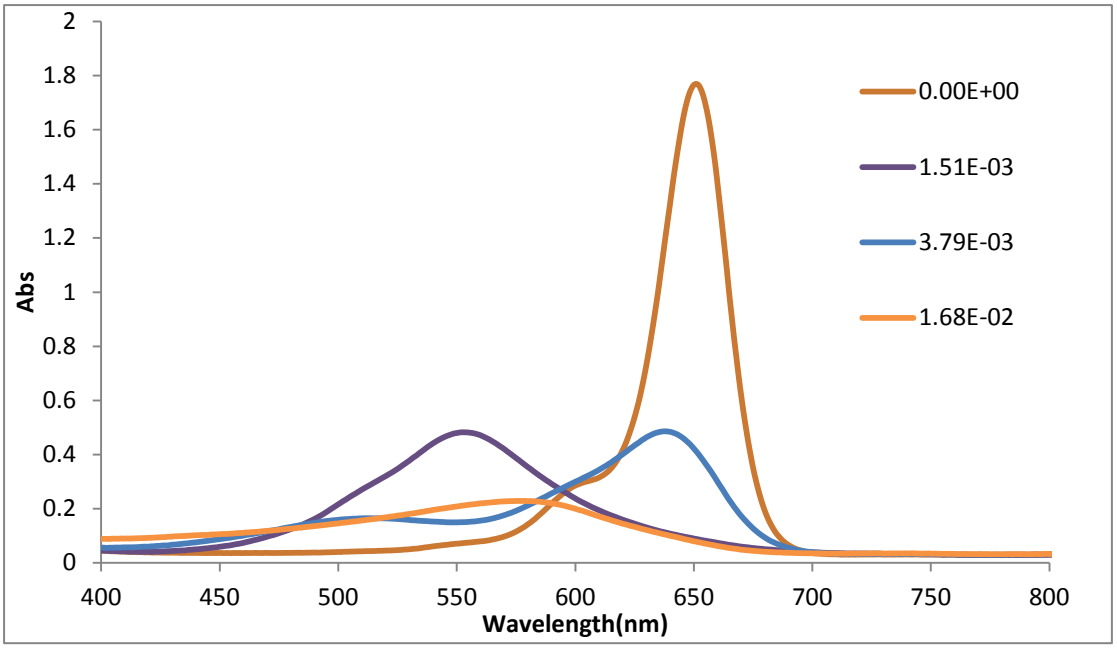

Figure 7.3: Absorbance spectra of $DiPSQ(OH)_2$ and three de-proton species in DMA.

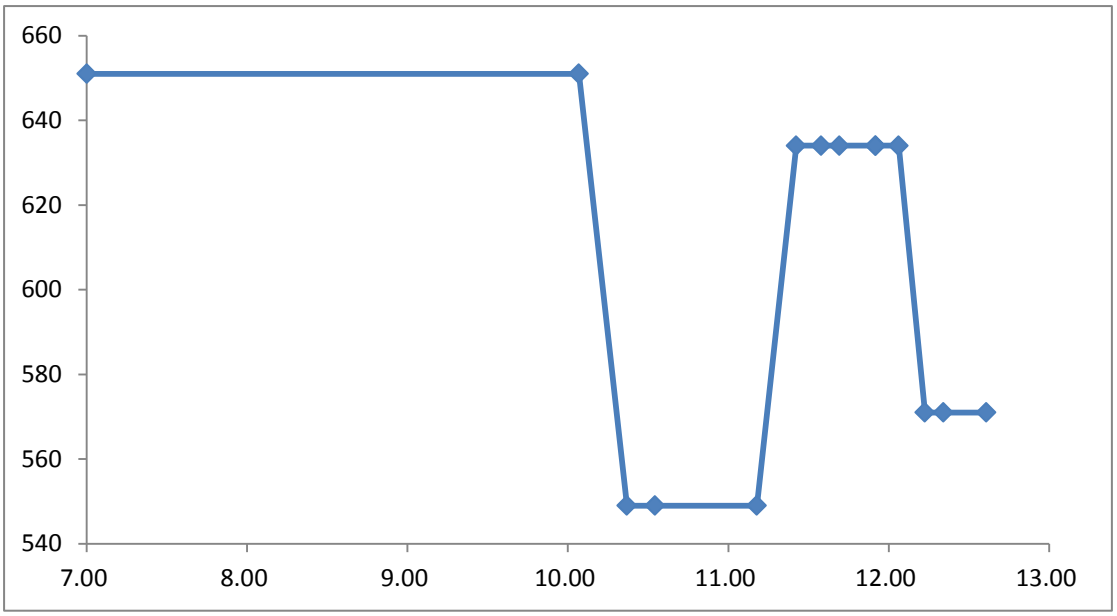

Figure 7.4: Variation of λ_{max} of absorption spectra of $DiPSQ(OH)_2$ as a function of PH.

7.4 Conclusion:

The sensitivity of $DiPSQ(OH)_2$ on pH is studied. Three deprotonated anions of DiPSQ(OH)2 are assigned by UV-VIS spectrometry: $DiPSQ(OH)_2^{-}$, $DiPSQ(OH)_2^{2-}$, and $DiPSQ(OH)_2^{3-}$. Absorption spectra of $DiPSQ(OH)_2$ vary as PH varies, and thus this dye can be used as a pH indicator. Also, this is helpful on device making. Now pH is a

factor that must be considered. Is a de-protonated species beneficial for OPV devices, and how do they behave in aggregation? These questions could be interesting in future studies.

Chapter 8

Summary

Squaraine dyes which absorb in the NIR spectrum have potential to improve the efficiency of OPV solar cell. Characterization of the photophysical properties of squaraine dyes is going to help us find the best material for the device. Photophysical properties (absorbance spectrum, extinction coefficient, emission spectrum, quantum yield, and fluorescence life time) of three new squaraine dyes ($DiBSQ(OH)_2$, $DiPSQ(OH)_2$, $DESQ(OH)_2$) were characterized in this paper. As the most interesting property of squaraines, aggregation is important because it broadens the range of absorption spectra. We believe that the side groups play a crucial role in aggregation; the smaller the side groups are, the bigger the excited state splitting will be, and the absorption range becomes wider as a result. Yet, $DiPSQ(OH)_2$ has the longest side N-alkyl chain, and it gives the most broadened absorption range in three squaraines. This feature makes $DiPSQ(OH)_2$ the most promising for OPV device, at least in the aspect of gathering most photons, while piquing interest as to why the alkyl group is so special. Aggregation also affects fluorescence. We conclude that aggregation is a strong quencher, which is the reason why solid state squaraine is non-fluorescent. Quantum yield data indicates that interactions exist between PCBM and squaraine, these interactions, either complex formation or aggregate enhancement, might be the reason why devices work despite zero quantum yield. For aggregates of $DiPSQ(OH)_2$, it is specified as dimer by research of in solutions.

For future research, it is valuable to focus on aggregation. The impact of aggregate of squaraines and the interaction between PCBM and squaraines on exciton diffusion needs to be addressed. Can we control aggregation by varying conditions in spin casting, such as using different solutions, different temperatures, or different ways of

annealing? Can we control aggregation by using different side groups? It is essential to understand how the device works for the purpose of optimizing their efficiency.

References

1 Tang, C. W. *Appl. Phys. Lett.* **1986**, *48*, 183.
2 Sariciftci, N. S.; Smilowitz, L.; Heeger, A. J.; Wudl, F. *Science* **1992**, *258*, 1474.
3 Serap Gunes, Helmut Neugebauer, Niyazi Serdar Sariciftci; *Chem. Rev*. **2007**, 107, 1324-1338.
4 Nunzi, J. M. C. R. *Physique.* **2002**, 3, 523.
5 B.A. Gregg and M.C. Hanna, *J. Appl. Phys.* **93** (2003) p. 3605.
6 Brian A. Gregg, *MRS Bulletin.* **2005**, 30, 20-22.
7 P. Peumans, S. Uchida, and S.R. Forrest, *Nature* **425** (2003) p. 158.
8 Stephen R. Forrest. *MRS Bulletin*. **2005**, 30, 28-32.
9 Ramamurthy, V., *Organic Photochemistry*. **1997**, p. 519-582.
10 Schmidt, A. H. Oxocarbons, R. West, Ed.;Academic Press: New York, **1980**.
11 Bigelow, R. W.; Freund, H. J. *Chem. Phys*. **1986**, 107, 159.
12 Bigelow, R. W.; Freund, H. J. *Chem. Phys.* **1986**, 107-159.
13 Law, K. Y. *Chem. Rev.* **1993**, 93, 449.
14 Merritt, V. Y.; Hovel, H.J. *Appl. Phys. Lett.* **1976**, 29, 414.
15 Jipson, V. P.; Jones, C. R. J. *Vac. Sci. Technol*. **1981**, 18, 105.
16 Mori, T.; Miyachi, K.; Kichimi, T.; Mizutani, T. *Jpn. J. Appl. Phys.* **1994**, 33, 6594.
17 Chen, C. T.; Marder, S. R.; Cheng, L. T. *J. Am. Chem. Soc.* **1994,** 116, 3117.
18 Sanghyun Paek, Hyunbong Choi, Chulwoo Kim, Nara Cho, Seulgi So, Kihyung Song, Mohammad K. Nazeeruddin, Jaejung Ko. *Chem. Commun.* **2011**, 47, 2874-2876.
19 Bernhard Oswald, Leonid Patsenker, Josef Duschl, Henryk Szmacinski, Otto S. Wolfbeis, Ewald Terpetschnig. *Bioconjugate Chem*. **1999**, 10, 925−931.
20 Padinger, F.; Rittberger, R.; Sariciftci, N. S. *Ad*V. *Funct. Mater.* **2003**, *13*, 85.
21 M Kasha, HR Rawls, MA El-Bayoumi. *Pure Appl. Chem*. **1965**, 371-392.
22 Principles of Fluorescence Spectroscopy_Lakowicz.pdf
23 Andrew Gilbert, Jim Baggott; *Essentials of Molecular Photochemistry*; Blackwell Scientific Publications. **1991**, p9.
24 Richard R. Lunt, Noel C. Giebink, Anna A. Belak, Jay B. Benziger, Stephen R. Forrest. *J. Appl. Phys*. **2009**, 105, 053711.
25 Richard R. Lunt, Jay B. Benziger, Stephen R. Forrest. *Advanced Materials*. **2010**, 22, 1233-1236.
26 Wingard, R. E. ***IEEE Ind. Appl.*** 1982,37,1251.
27 Tristani-Kendra, M.; Eckhardt, C. J. ***J. Chem. Phys.*** 1984,81,1160.
28 Brian A. Gregga, Mark C. Hanna. *J. Appl. Phys*. **2003**, 93, 6.
29 Minquan Tian, Makoto Furuki, Izumi Iwasa, Yasuhiro Sato, Lyong Sun Pu, Satoshi Tatsuura. *J. Phys. Chem. B* **2002**, 106, 4370–4376.
30 *Techical note - Time-Correlated Single Photon Counting*, from **PicoQuant**.
31 *F-3018 PLQY integrating sphere accessory - Methodology*, from **HORIBA Jobin Yvon**.
32 Law, K. Y. *J. Phys. Chem.* **1987,** 91, 5184.
33 Law, K. Y. *J. Photochem. Photobiol. A: Chem*. **1994,** 84, 123.
34 Bigelow, R. W.; Freund, H. J, *Chem. Phys*. **1986**, 107, 159.
35 Kamlet, M. J.; Abboud, J. L.; Taft, R. W. *J. Am. Chem. Soc*. **1977**, 99, 6027.
36 Law, K. Y. *J. Phys. Chem*. **1989**, 93, 5925.

37 D. E. Bornside, C. W. Macosko, L. E. Scriven. *J. Electrochem. Soc*. **1991**, 138, 317-320.
38 Kangning Liang, Kock-Yee Law, David G. Whitten. *J. Phys. Chem.* **1994,** *98,* 13379-13384.
39 Yongqian Xu, Zhiyong Li, Andrey Malkovskiy, Shiguo Sun and Yi Pang. *J. Phys. Chem. B.* **2010**, 114 (25), 8574–8580.
40 Andrew Gilbert, Jim Baggot. *Essentials of Molecular Photochemistry*. **1991**, P103.
41 Benesi, H.; Hildebrand, J. H. *J. Am. Chem. Soc*. **1949**, *71*, 2703.
42 J. Griffiths, J. Mama. *Dyes and Pigments*. **2000**, 44, 9-17.